HHS Public Access

Author manuscript

J Neurochem. Author manuscript; available in PMC 2023 June 01.

Published in final edited form as:

J Neurochem. 2022 June ; 161(5): 435–452. doi:10.1111/jnc.15612.

Developmental, neurochemical and behavioral analyses of ErbB4 Cyt-1 knockout mice

Larissa Erben[1], **Jacqueline P. Welday**[1], **Marie E. Cronin**[1,2], **Ricardo Murphy**[1], **Miguel Skirzewski**[1,3], **Detlef Vullhorst**[1], **Steven L. Carroll**[4], **Andres Buonanno**[1,5]

[1]Section on Molecular Neurobiology, Eunice Kennedy Shriver National Institute of Child Health and Human Development, National Institutes of Health, Porter Neuroscience Research Center, Bldg. 35, Room 2C-1000, Bethesda, MD 20892, USA

[2]current: Neurobiology, Duke University, Durham, NC 27701, USA

[3]current: Rodent Cognition Research and Innovation Core, Western University, London, Ontario N6A5B7, Canada.

[4]Department of Pathology and Laboratory Medicine, Medical University of South Carolina, Charleston, SC 29425, USA

Abstract

Neuregulins (NRGs) and their cognate neuronal receptor *ERBB4*, which is expressed in GABAergic and dopaminergic neurons, regulate numerous behaviors in rodents and have been identified as schizophrenia at-risk genes. ErbB4 transcripts are alternatively spliced to generate

[5]**Corresponding author:** Andrés Buonanno, Ph.D., Section on Molecular Neurobiology, Eunice Kennedy Shriver National Institute of Child Health and Human Development (NICHD), National Institutes of Health (NIH), Bethesda, MD 20892-3713, buonanno@mail.nih.gov.

Author Contributions: LE and AB designed this study. Funding provided by AB and SLC. LE, MEC, RM and JPW carried out surgical and behavioral experiments. LE, DV and MS carried out chemical and biochemical experiments. Mice were generated by DV and SLC. LE, MEC, MS, JPW and AB analyzed data. LE, JPW and AB wrote the manuscript. All authors provided critical feedback and contributed to the final manuscript.

Conflicts of Interest

Andrés Buonanno is a senior editor for the Journal of Neurochemistry. No additional conflicts of interest to report.

Data Availability

Data are available from the author upon reasonable request.

--Human subjects --

Involves human subjects:

If yes: Informed consent & ethics approval achieved:

=> if yes, please ensure that the info “Informed consent was achieved for all subjects, and the experiments were approved by the local ethics committee.” is included in the Methods.

ARRIVE guidelines have been followed:

Yes

=> if it is a Review or Editorial, skip complete sentence => if No, include a statement in the “Conflict of interest disclosure” section: “ARRIVE guidelines were not followed for the following reason:“

(edit phrasing to form a complete sentence as necessary).

=> if Yes, insert in the “Conflict of interest disclosure” section:

“All experiments were conducted in compliance with the ARRIVE guidelines.” unless it is a Review or Editorial

Conflicts of interest: A.B. is a senior editor for the Journal of Neurochemistry. No additional conflicts of interest to report.

=> if ‘none’, insert “The authors have no conflict of interest to declare.”

=> else insert info unless it is already included

Open Science Badges

No, I am not interested to achieve Open Science Badge(s) => if yes, please see Comments from the Journal for further information => if no, no information needs to be included in the manuscript.

isoforms that either include (Cyt-1) or exclude (Cyt-2) exon 26, which encodes a cytoplasmic domain that imparts ErbB4 receptors the ability to signal via the phosphoinositide 3-kinase (PI3K)/protein kinase B (Akt) pathway. Although ErbB4 Cyt-1/2 isoforms have been studied in transfected cultured cells, their functions *in vivo* remain unknown. Here we generated ErbB4-floxed (ErbB4-Cyt1$^{fl/fl}$) mice to investigate the effects of germline (constitutive) and conditional (acute) deletions of the Cyt-1 exon. Overall receptor mRNA levels remain unchanged in germline ErbB4 Cyt-1 knockouts (Cyt-1 KOs), with all transcripts encoding Cyt-2 variants. In contrast to mice lacking all ErbB4 receptor function, GABAergic interneuron migration and number are unaltered in Cyt-1 KOs. However, basal extracellular dopamine (DA) levels in the medial prefrontal cortex are increased in Cyt-1 heterozygotes. Despite these neurochemical changes, Cyt-1 heterozygous and homozygous mice do not manifest behavioral abnormalities previously reported to be altered in ErbB4 null mice. To address the possibility that Cyt-2 variants compensate for lack of Cyt-1 during development, we microinjected an adeno-associated virus expressing Cre-recombinase (AAV-Cre) into the DA-rich ventral tegmental area of adult ErbB4-Cyt1$^{fl/fl}$ mice to acutely target exon 26. These conditional Cyt-1 KOs were found to exhibit behavioral abnormalities in the elevated plus maze and startle response, consistent with the idea that late exon 26 ablation may circumvent compensation by Cyt-2 variants. Taken together, our observations indicate that ErbB4 Cyt-1 function *in vivo* is important for DA balance and behaviors in the adult.

Graphical Abstract

ErbB4 receptor transcripts are alternatively spliced to generate Cyt-1 or Cyt-2 isoforms. Cyt-1 isoforms include exon 26, which render ErbB4 receptors the ability to signal via the PI3K/Akt pathway. We found that mice constitutively lacking exon 26 exhibit a dopamine imbalance but few behavioral deficits. To address the possibility that Cyt-2 variants compensate for lack of Cyt-1 during development, we microinjected AAV-Cre into the dopamine-rich mesencephalon of adult ErbB4-Cyt1$^{fl/fl}$ mice to acutely target exon 26. These conditional Cyt-1 KOs exhibit behavioral alterations in the elevated plus maze and startle response.

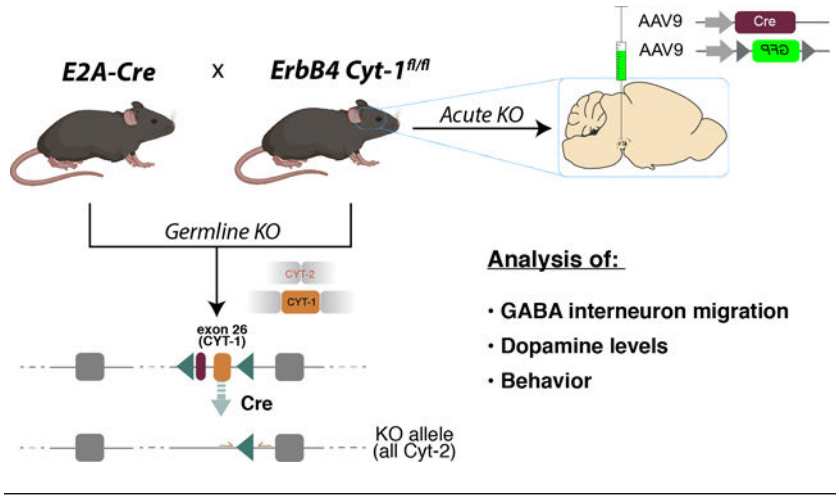

Introduction

The Neuregulin (NRG) family of neurotrophic factors, as well as their cognate neuronal receptor tyrosine kinase ErbB4, are genetically associated with a risk for schizophrenia (Scz) and its endophenotypes (Stefansson et al. 2002; Silberberg et al. 2006; Greenwood et al. 2012; Mei & Nave 2014; Mostaid et al. 2016; Buonanno 2010). NRG/ErbB4 signaling is best characterized in the cortex and hippocampus, where ErbB4 expression is confined to GABAergic interneurons, (Vullhorst et al. 2009; Fazzari et al. 2010), as well as in the mesencephalon, where ErbB4 is highly expressed in dopaminergic (DAergic) neurons (Steiner et al. 1999; Abe et al. 2009; Skirzewski et al. 2018). Germline ablation of ErbB4 results in embryonic lethality due to failure of heart trabeculation (Gassmann et al. 1995), which can be circumvented by selective transgenic expression of ErbB4 in the heart (Tidcombe et al. 2003). Using heart-rescued ErbB4 null mice, NRG/ErbB4 signaling has been shown to regulate the migration, allocation and number of cortical GABAergic interneurons during embryonic and neonatal development (Flames et al. 2004; Bartolini et al. 2017; Neddens & Buonanno 2010). Later in development, NRG/ErbB4 signaling regulates the maturation of glutamatergic synapses onto GABAergic interneurons (Woo et al. 2007; Fazzari et al. 2010; Yang et al. 2013; Del Pino et al. 2013; Yang et al. 2018; Vullhorst et al. 2015; Kotzadimitriou et al. 2018), particularly parvalbumin (PV)-positive fast-spiking interneurons, that modulate critical period plasticity (Sun et al. 2016; Gu et al. 2016) and neuronal network activity (Fisahn et al. 2009; Nason et al. 2011; Andersson et al. 2012). NRG/ErbB4 signaling in midbrain DAergic neurons also regulates DA homeostasis and cognitive function (Kwon et al. 2008; Skirzewski et al. 2018; Skirzewski et al. 2020; Yan et al. 2018; Namba et al. 2016). Interestingly, both NRG2 and ErbB4 KOs, as well as conditional ErbB4$^{fl/fl}$ mutant mice that lack the receptor in tyrosine hydroxylase (Th)-expressing neurons (Th-Cre; ErbB4$^{fl/fl}$), exhibit imbalances of basal extracellular DA levels in distinct projection areas (Skirzewski et al. 2018; Skirzewski et al. 2020; Yan et al. 2018; Kato et al. 2011; Mizuno et al. 2013) that are reminiscent of the imbalances in DA release reported in dorsal striatum and dorsolateral prefrontal cortex (DLPFC) of Scz patients (Slifstein et al. 2015; Weinstein et al. 2017). Consistent with the association of the NRG/ErbB4 signaling pathway with a risk for Scz, mice with targeted mutations in either *nrg1*, *nrg2*, *nrg3* or *erbb4* manifest many behavioral abnormalities that are associated with traits observed in Scz (Chen et al. 2010; Muller et al. 2018; Skirzewski et al. 2018; Tan et al. 2018; Hayes et al. 2016; Lu et al. 2014; Shamir et al. 2012; Wen et al. 2010; Yan et al. 2018), and in some studies shown to be ameliorated by antipsychotic treatment (Tan et al. 2018; Yan et al. 2018). In addition to having altered levels of extracellular dopamine (Skirzewski et al. 2018), ErbB4 null mice are hyperactive, exhibit anxiety-like behaviors on the elevated plus maze, have reduced pre-pulse inhibition (PPI) responses to startle and perform poorly relative to wild-type littermates in numerous tasks (i.e., T-, Y- and Barnes-maze) that require hippocampal/prefrontal cortical functions (Shamir et al. 2012; Skirzewski et al. 2020; Wen et al. 2010).

Members of the ErbB receptor family (ErbB1-ErbB4) are type-I transmembrane proteins comprised of an extracellular NRG-binding domain and an intracellular tail encoding a tyrosine kinase and regulatory binding sites necessary for downstream signaling. NRG

binding to ErbB3 or ErbB4 receptors promotes their heteromeric or homomeric dimerization to initiate MAPK or phosphatidylinositol-3-kinase (PI3K)/Akt downstream signaling. In the brain, ErbB4 is the major neuronal NRG receptor (reviewed by (Buonanno & Fischbach 2001; Mei & Nave 2014). Whereas several studies have investigated the consequences of ablating ErbB4 on the functions of cortical/hippocampal GABAergic interneurons and DAergic neurons, relatively little is known about the selective functions of different ErbB4 splice variants. Four ErbB4 isoforms are generated by alternative splicing of exons encoding sequences in either the extracellular juxtamembrane (JM) domain (exon 16) that encodes a cleavage site for metalloproteases, or at the cytoplasmic (Cyt) domain where inclusion or exclusion of exon 26 generates ErbB4 Cyt-1 and Cyt-2 isoforms, respectively (Elenius et al. 1997; Elenius et al. 1999). The additional 16 amino acids encoded by exon 26 of Cyt-1 receptor variants form a docking site for PI3K and a recognition motif for WW domain proteins (PPXY) (Elenius et al. 1999; Omerovic et al. 2004). As a result, Cyt-1-containing ErbB4 receptors can directly stimulate PI3K and Akt phosphorylation (Elenius et al. 1999; Kainulainen et al. 2000). By contrast, ErbB4 Cyt-2 subunits require heterodimerization with either ErbB3 (also activates PI3K) or ErbB4 Cyt-1 subunits to initiate downstream PI3K/Akt signaling (Gambarotta et al. 2004). Interestingly, in the postmortem DLPFC of Scz patients, the ratio of ErbB4 Cyt-1/Cyt-2 variants and the downstream target PI3KCD are increased compared to healthy controls (Silberberg et al. 2006; Law et al. 2007; Law et al. 2012; Joshi et al. 2014; Chung et al. 2016), suggesting a selective association of the ErbB4 Cyt-1 isoform with risk for Scz.

Both convergent and divergent biological functions have been reported for ErbB4 Cyt-1 and Cyt-2 isoforms based on experiments performed in non-neuronal cell lines (reviewed in (Veikkolainen et al. 2011)). In most regions of the CNS, Cyt-2 accounts for approximately 60% of total ErbB4 transcripts, whereas Cyt-1 variants predominate (~80%) in the heart (Veikkolainen et al. 2011; Chung et al. 2016; Erben et al. 2018). Several studies have suggested ErbB4 isoform-specific functions in the CNS (Gambarotta et al. 2004; Fregnan et al. 2011; Fornasari et al. 2016; Veikkolainen et al. 2011), including GABAergic interneuron migration during embryonic and postnatal development *in vivo* (Rakic et al. 2015). However, the relative contribution of Cyt-1 receptor isoforms to the numerous aforementioned functions attributed to ErbB4, based on studies using ErbB4 null mice, remains unknown. To investigate the specific functions of ErbB4 Cyt-1 on GABAergic and DAergic pathways *in vivo*, we generated ErbB4 Cyt-1 knockout (KO) mice using Cre/*loxP* site-directed homologous recombination to selectively target exon 26 either by germline deletion (EIIa-Cre;ErbB4 Cyt-1$^{fl/fl}$ mice) or by acute ablation in the adult animals using adeno-associated virus expressing Cre-recombinase (AAV-Cre) microinjections in Cyt-1$^{fl/fl}$ mice.

Methods:

Time-line of the study design, experimental procedures and number of mice used: see Fig. S1. *Animals & generation of Cyt-1 KOs*

Mice were kept on a 12h-12h light-dark schedule with access to food and water *ad libitum*. All studies were conducted in female and male mice during the light cycle.

Animals were handled in accordance with the NIH Animal Welfare guidelines and all animal procedures were approved by the NIH Animal Care and Use Committee (ASP #18–074). The Cyt-1 targeting construct, harboring loxP sites flanking ErbB4 exon 26, was generated by "recombineering" using vector pL253 (Liu et al. 2003) (Fig. 1A). Site-specific recombination of the *erbb4* locus and generation of conditional Cyt-1 mutant mice was performed at the Transgenic & Genetically Engineered Models Core of the University of Alabama at Birmingham. Successfully targeted and PCR-validated embryonic stem (ES) cells derived from C57BL/6J mice (Li et al. 2016) were injected into blastocysts from albino C57BL/6J mice (JAX stock # 000058). Chimeric offspring were bred with albino C57BL/6J mice; only black F1 mice were used for further breeding. Mice were then crossed to FLP deleter strain B6;SJL-Tg(ACTFLPe)9205Dym/J (JAX stock # 003800) to remove the FRT-flanked neomycin cassette used for ES cell selection. Null (germline) Cyt-1 mutant mice, hereafter referred as Cyt-1 knockouts (KOs), were generated by crossing floxed Cyt-1 mice to mice expressing Cre recombinase under the control of ubiquitously active EIIa promoter (also on C57BL/6 background; JAX stock # 003724). Heterozygous Cyt-1 mice were used for breeding and yielded normal litter sizes (6.4 pups ± 0.11, N=2 cohorts, n=648 mice; compared to C57BL/6J 6.2 ± 0.2 pups (Nagasawa et al. 1973)), balanced sexes (52.9 ± 1.29% males, N=2 cohorts, n=648 mice), and Mendelian genotype frequencies (24.5 ± 0.03% +/+, 50.3 ± 1.47%, 25.1 ± 1.44%, N=2 cohorts, n=648 mice). Routine genotyping was performed by PCR using forward primers 5'-AGTTTCCTTATTCCTAGCTCTCC-3' and 5'-TGTCTTAGATGTCTGTAACTTGG-3' and reverse primer 5'-GATGATCCAGCAATGCTACCCTC-3' at 60°C annealing for 20s and 72°C elongation for 10s. Primer binding sites are schematically illustrated in Fig. 1A and representative genotyping results are shown in Fig. 1B. Cyt-1 KOs were crossed to GAD67-GFP mice (Tamamaki et al. 2003) to analyze GABAergic interneuron density by immunohistochemistry in GFP+/− mice (denoted as Cyt-1 KO; GAD-GFP, see below). Adult wild-type C57BL/6J mice were obtained from Jackson Laboratory. This study was not preregistered.

Isoform-specific in situ hybridization (ISH)

Exon-specific ISH (BaseScope version 1 & 2; Advanced Cell Diagnostics) was performed on coronal formalin-fixed paraffin-embedded serial 8 μm-sections of 8–11 week-old adult mice (C57BL/6J or Cyt-1 homozygote/heterozygote mutants and control littermates; both sexes) as previously described (Erben et al. 2018; Erben & Buonanno 2019). ErbB4 Cyt-1 and Cyt-2 probes were custom-made to respectively target mouse ErbB4 exon junctions 25/26 (5'-CATCTACACATCCAGAACAAGAATTGACTCCAATAGG/AGTGAAATTGGAC-3') and 25/27 (5'-CCATCTACACATCCAGAACAAGAATTGACTCCAATAGG/AATCAGTTTGT-3'). Briefly, paraffin sections were deparaffinized with xylene and pretreated with hydrogen peroxide (10 min at RT), antigen-retrieved (15 min at 100°C) and incubated with proteases (protease III, 30 min at 40°C). Next, probes were incubated for 2 h at 40°C, the signal was chemically amplified with 7/8 amplification steps (BaseScope version 1/2) and subsequently detected using alkaline phosphatase and FastRED dye. For post-hoc immunostaining, sections were immediately labeled with rat anti-DA transporter (DAT) antibody (clone 6–5G10; Santa Cruz; catalog # sc-32258; 1:200)

followed by secondary donkey anti-rat antibody conjugated to Alexa 488 (1:1000, Thermo Fisher; catalog # A-21208) as described (Erben & Buonanno 2019), using standard immunofluorescence histochemistry (IHC) protocol (see below).

Immunofluorescence histochemistry (IHC)

Immunostaining of 50 μm-thick free-floating sections of postnatal day 30 (P30) Cyt-1 KO; GAD-GFP and heterozygote/controls (n=4, both sexes) was performed as previously described (Vullhorst et al. 2017). Briefly, mice were euthanized using an overdose of anesthetic Avertin and transcardically perfused with 4% paraformaldehyde (PFA) in 0.1M phosphate-buffered saline, pH 7.4. Dissected brains were post-fixed overnight in the same fixative at 4°C and 50 μm-thick serial sections cut on a vibratome. Sections were blocked in 10% normal donkey serum, 0.3% Triton X-100 in 0.1 M PBS for 1 h at RT and incubated with primary antibodies in blocking solution overnight at 4°C. Following three 10 min washes in 0.1 M PBS with 0.25% Triton X-100, sections were incubated with secondary antibodies in blocking buffer for 2h at RT. Sections were extensively washed with 0.1 M PBS, counterstained with DAPI and mounted with Mowiol-DABCO. Primary antibodies were rat monoclonal anti-GFP (clone GF090R, Nacalai Tesque, Japan; catalog # 04404–84; 1:2000), chicken anti-GFP (Life technologies, catalog # A10262; 1:2000), rabbit anti-TH (Pel Freez; catalog # P40101; 1:3000) and rat monoclonal DAT (clone 6–5G10, Santa Cruz; catalog # sc-32258; 1:200), which were visualized with secondary antibodies raised in donkey (Invitrogen, Thermo Fisher & Jackson Immuno Research). For GABAergic interneuron densities, bilateral cortical analyses were performed at three different bregma levels (~+0.26, −0.46, −1.22), and bilateral hippocampal analyses at four different bregma levels (~−1.22, −1.82, −2.46, −3.08). Damaged sections were excluded from analysis (n=6 bregma locations excluded due to damage).

Image analysis

Fluorescent FastRED ISH signals were analyzed at 20x magnification using Zeiss LSM710/800 confocal microscopes. Unbiased automated quantitative analysis of maximum intensity projections obtained from Z-stack images was performed using CellProfiler (Carpenter et al. 2006), as previously described (Erben et al. 2018). For ISH-IHC analyses, >30% overlap of the cell with DAT staining was used to define a neuron as DAergic. Similarly, IHC in GAD-GFP mice was analyzed at 10x magnification using a Zeiss LSM800 confocal microscope. Density of GABAergic interneurons was analyzed from maximum intensity projections using a custom-made CellProfiler pipeline to identify GAD-GFP+ cells (size >25 μm^2 (SSCtx) or 50 μm^2 (Hpp); threshold=1.5x median background intensity; eccentricity >0.94). Hippocampal subregions and cortical layers were defined based on morphology, DAPI stain and interneuron density. Injection sites in floxed Cyt-1 mutant mice were verified at 10x magnification using a Zeiss LSM800 confocal microscope (see below). For all analyses, areas examined were not different between transcripts and/or genotype or group.

Quantitative reverse-transcription PCR (RT-qPCR)

Real-time RT-qPCR using TaqMan probes was performed as previously described (Erben et al. 2018). Briefly, whole brain (n=3/genotype) and hippocampal (n=4/genotype) total

RNA was isolated from male and female ten-week-old Cyt-1 heterozygote, null and WT littermates using TRI Reagent (Thermo Fisher; catalog # AM9738). cDNA was synthesized from 1 μg RNA using SuperScript IV Reverse Transcriptase (Thermo Fisher; catalog #18090050) and random hexamers for 20 min at 55°C. Gene expression was subsequently assessed using TaqMan universal PCR Master Mix (Thermo Fisher; catalog #4304437), 0.25 μM FAM/VIC-labeled TaqMan probes, and 0.9 μM primers from 2.5–5 ng cDNA in a total volume of 10 μl. Cycling was performed in 384-well plates using a QuantStudio 6 Thermocycler (Thermo Fisher) and the following parameters: 2 min at 50°C and 10 min at 92°C, followed by 40 cycles of 15 s at 95°C, 1 min at 65°C (for Cyt probes) or 60°C (for all other probes). Custom-made isoform-specific ErbB4 TaqMan probes (Thermo Fisher) were FAM-ATGGACGGGCCATTCCACTTTACCA-MGB for JMa, FAM- TTCAAGCATTGAAGACTGCATCGGCCTGAC-MGB for JMb, FAM-TGAAATTGGACACAGCCCTCCTCCTG-MGB for Cyt-1 and FAM-AATTGACTCCAATAGGAATCAGTTTGTGTACCAAGAT-MGB for Cyt-2. Flanking primers were 5'-CCACCCTTGCCATCCAAA-3' and 5'-CCAATGACTCCGGCTGCAATCA-3' for JM isoforms, and 5'-CAACATACCTCCTCCCATCTACAC-3' and 5'-GCATTCCTTGTTGTGTAGCAAA-3' for Cyt isoforms. ErbB3 (Thermo Fisher, Mm01159999_m1) and ErbB4 (Thermo Fisher, Mm01256793_m1) TaqMan probes were commercial. A VIC-labeled TaqMan probe for GAPDH (Thermo Fisher, Mm9999915_g1) was used for normalization. Standard curves (10 ag–1 ng) of cloned DNA for ErbB4 JMa/Cyt-1 and JMb/Cyt-2 and of a synthetic DNA fragment for ErbB3, confirmed linearity and showed similar amplification efficiencies for isoform-specific assays. Assay specificity was tested using 100 pg DNA of non-matching ErbB4 isoforms or ErbB receptor.

DA measurements.

Basal extracellular DA levels in the medial prefrontal cortex (mPFC) of freely moving mice (n=6–7/genotype, both sexes, 2.5–4 months old) were measured using the no-net flux (NNF) microdialysis approach (Friend et al. 2017). Mice were anesthetized using aerosolized isoflurane first at a 3% flow rate for a 5-minute induction period and then maintained throughout surgery at 1.5–2% flow rate. Briefly, counterbalanced unilateral stainless-steel guide shafts (21-gauge, 6mm-long) were chronically implanted into the mPFC (AP:2.0mm, L:0.3mm, V:0.3 mm with respect to bregma). One week after surgery NNF measurements were made after lowering a laboratory-made microdialysis probe through the implanted guide shaft as reported (Hernandez et al. 1986). The tip of the microdialysis probe consisted of a 2 mm-long cellulose hollow fiber (18 kDA MWCO, SpectrumLabs Inc) protruding from the tip of the guide shaft. Artificial cerebrospinal fluid (aCSF; 136 mM NaCl, 3.7 mM KCl, 2.2 mM $CaCl_2$, 1 mM $MgCl_2$, and 10 mM $NaHCO_3$ at pH 7.4) was continuously perfused through the microdialysis probe at a flow rate of 1 μl/min for 2 h before sample collection. Five different DA standard concentrations (0, 0.5, 1.0, 1.5, and 2.0 nM) were randomly perfused for 60 min through the microdialysis probe and duplicate 30-min samples per standard were collected in 10 μl of 100 mM HCl + 1 mM EDTA to prevent catecholamine degradation. Samples were immediately frozen and stored at −80°C until subsequent analysis within a week. Probe placements were verified by Nissl staining in 50-μm thick vibratome sections (Fig. 5A); animals with misplaced probes were excluded from

analysis. DA standards and samples were injected using a HPLC autosampler (INSIGHT, Eicom) into an isocratic HPLC system coupled to amperometric detection according to the manufacturer's instructions (HTEC-510, Eicom). Regression curves were generated by subtracting the area under the curve of the corresponding standard (IN) minus the area under the curve of the dialysate sample (OUT). Regression equations were used to estimate the NNF DA concentration (at y=0) for each mouse.

Stereotaxic injections

Adult male and female 3- to 4-month-old Cyt-1$^{fl/fl}$ mice were used for stereotaxic bilateral mesencephalic microinjections. To acutely target ErbB4 Cyt-1$^{fl/fl}$ recombination and visualize the transduced neurons, AAV-Cre (serotype 9; pENN.AAV.hSyn.Cre.hGH, Addgene; catalog # 105555, Lot: v35950) was mixed with DIO-GFP (pAAV.synP.DIO.EGFP.WRPE.hGH, Addgene; catalog #100043, Lot: v25058) at 1.0×10^10 GC/mL (Cre) and 3.0×10^12 GC/mL (DIO-GFP) in sterile PBS. As controls, mice were microinjected with 3.0×10^12 GC/mL AAV-GFP (pAAV.hSyn.eGFP.WRPE.bGH, Addgene; catalog # 105539, Lot: 38081) diluted in sterile PBS. Cyt-1$^{fl/fl}$ mice were anesthetized during surgery using isoflurane as described above. Equal numbers of Cyt-1$^{fl/fl}$ mice were microinjected with 200 nL of either AAV Cre/DIO-GFP or AAV-GFP at a flow rate of 5 nl/sec using the following stereotaxic coordinates: AP −2.7 mm (with respect to bregma), L ±0.75 mm (with respect to bregma), V −4.35/−4.3 mm (relative to brain surface; 100 nl/each Z) to target the VTA. Microinjections using glass capillaries (Drummond Nanoinjector) were performed for 8 min and capillaries left in place for an additional 2 min before withdrawing to avoid retrograde mass flow. Mice were allowed to recover and closely monitored for 2 weeks before they were used in behavioral tests and given i.p. ketoprofen injections (5 mg/kg) three consecutive days post-op to manage pain. Upon completion, injection sites were verified by immunostaining using anti-GFP, and markers for DAergic neurons anti-DAT and anti-TH antibodies; mis-injected mice were excluded from analyses (n=4 mice excluded from analyses for misinjection).

Behavioral tests

Behavioral testing of conditional ErbB4 Cyt-1 KOs (3–7 months old) was conducted in the following sequence: open field, elevated plus maze, PPI, Y-maze and Barnes maze testing. Acute AAV-injected Cyt-1$^{fl/fl}$ mice (3 months old; both sexes) were tested as follows: in the open field, elevated plus maze, Y-maze and PPI. Behavioral testing was performed on multiple cohorts comprised of male and female mice during the light cycle and all apparatuses were cleaned with 70% ethanol between trials. Tracking in the open field and the elevated, Y and Barnes mazes were conducted with ANY-maze software. The experimenter was blind to the mouse genotypes except for behaviors performed with acute AAV-injected Cyt-1$^{fl/fl}$ mice.

Open Field: Mice (n=12–14/genotype) were habituated to the testing environment for 30 min prior to measuring locomotor activity in a 50 cm x 50 cm x 30 cm white chamber (the center was defined as 28 cm x 28 cm, 70–80 lux in the perimeter, 80–90 lux in the center). Mice were permitted to freely explore the maze for 30 min, and the traveled distance and time spent in the center were recorded.

Elevated plus maze: The elevated plus maze test for anxiety-like behavior was performed in a plus-shaped white plastic apparatus (30 cm x 5 cm arms) consisting of two closed arms (18 cm-high black walls, 60–70 lux) and two open arms (130–140 lux) elevated 40 cm above the ground. ErbB4 Cyt-1 mutant and WT controls (n=11–14/genotype) were habituated for 30 min prior to testing. Mice were permitted to explore the maze for 5 min and time spent in the open and closed arms was recorded.

PPI: Startle reflex and PPI were measured in a SR-LAB-Startle Response System (San Diego Instruments, San Diego, CA). ErbB4 Cyt-1 mutant mice (n=17–18/genotype) were habituated to a 65 dB background noise in the plexiglass tube of the testing chamber for 5 min on 3 consecutive days. Startle reflex was measured by pseudo-random presentations of tones ranging from 70 to 120 db (5 db increments, 5 tones each) and normalized to the average startle response to 120 db pulses of the entire cohort. During PPI testing on the following day, animals were presented with a pseudorandom sequence of 20 ms pre-pulse tones (PP; 66, 70, 74, 78 dB; 12 times each) and 40 ms 120 dB pulse pairings with variable inter-trial interval between 10 to 45 s. A 120 db no pre-pulse (NPP) presented 28 times was used to calculate the percentage of PPI of startle response as [(average startle to NPP – average startle to PP)/average startle to NPP]*100.

Y-maze: Working memory was tested in Cyt-1 mutant mice (n=12–14/genotype) using a Y-maze apparatus (30 cm x 18 cm x 9.5 cm three-arm maze with opaque tan walls, 50 lux). Mice were habituated for 30 min to the testing environment and then permitted to explore the maze for 5 min. Novel arm entries (spontaneous alternation) were identified as entries into the third arm different from the current and previously explored arm. Consecutive arm entry is considered as a single entry but accounted for total arm entries (Heredia-Lopez et al. 2016). Percentage of alternation was calculated as [(number of alternations)/(total arm entries-2)]*100.

Barnes maze: Barnes maze spatial learning and memory test was conducted as previously described (Skirzewski et al. 2018). The edge of the round elevated apparatus (Stoelting, 90 cm diameter, 800 lux, 90 cm above ground) was marked by 20 open holes (~10 cm diameter) with a hidden escape chamber placed underneath of one of the holes (target, 0) and the remaining holes labeled as +1 to +10, and −1 to −9. The edges of the maze were covered with a wall providing spatial cues and 85 db background white noise was played during all phases of the test. The Barnes Maze test consisted of three phases: training, probe test, and new escape test. During the training, mice (n=8–11/genotype) were allowed to explore the maze. The trial ended when the animal entered the escape chamber; at that point, the noise switched off automatically and aversive light was blocked. The mouse was held in the chamber for 1 min. Mice that could not locate the chamber within 3 min were manually guided to the escape hole. Training was conducted over four days (4 trials per day). Mice that failed to escape the maze in more than one trial on the fourth day of training were excluded from analysis. On the fifth day, the escape chamber was removed, and mice were tested for 90 s (probe test). Latency to escape and time in the correct zone were recorded using ANY-maze software (Stoelting Co, Wood Dale, IL), target hole nose pokes and errors defined as non-target nose pokes were quantified by hand-scoring of collected videos. Forty-

eight hours after the probe test, mice were re-introduced to the testing apparatus in which the escape chamber had been moved from its original position to hole +8 (new target test). Mice were permitted to explore the maze until they located the new escape for up to 3 min, at which point they were guided to the new escape (see learning phase). Four subsequent trials were performed and latency to escape and errors were quantified as described above.

Experimental Design & Statistical Analyses

Statistical analyses were performed using Graph Pad Prism 8 and JASP (Version 0.11.1). All data represent the mean ± SEM and statistical significance was set at $p<0.05$. Outliers (ROUT, Q=1%) were excluded from data analyses. All data sets were examined for normality using Shapiro-Wilk test and for equality of variance using Levene's/Mauchly's test and, if necessary, data was corrected using Welch's/Geisser-Greenhouse correction Statistical analyses were performed using one-way ANOVA/Welch's ANOVA/Kruskal-Wallis test and Tukey's/Dunnett's multiple comparisons test (Fig. 1C-E; Fig. 3G,H; Fig. 4A; Fig. 5B; Fig. 6A,D,E); paired nonparametric Wilcoxon test (Fig. 2C,D), or unpaired t-test (Fig. 7C) for comparison of two groups only and two-way ANOVA/mixed-effects analysis and Tukey's multiple comparison test for comparisons of multiple variables (Fig. 3I,J; Fig. 4B-D, Fig. 6B,C,F-H; Fig. 7B,D,E). Simple randomization was performed to assign animals to a group, groups were balanced for sex and within cages when applicable (Kim & Shin 2014). Given that Cyt-1 is a splice variant of ErbB4, requisite sample sizes were determined based on previous work in our lab studying animals with mutations in the Nrg/ErbB signaling pathway that had sufficient power to identify biologically significant phenotypes using approaches similar to those employed here (Shamir et al. 2012; Skirzewski et al. 2020; Wen et al. 2010); a *priori* power calculations were not performed.

Results:

Generation of Cyt-1 KO mice

Numerous studies have investigated the functions of ErbB4 receptors during early neurodevelopment and in the adult using heart-rescued ErbB4 null mice (Tidcombe et al. 2003; Shamir et al. 2012; Flames et al. 2004; Tan et al. 2018). However, because the specific *in vivo* functions of different receptor isoforms are presently unknown, we targeted exon 26 by Cre/*loxP* homologous recombination to investigate the role of ErbB4 Cyt-1 isoforms (see Materials & Methods, Fig. 1A). Initially, the *frt*-flanked neomycin cassette was removed by crossing founder mice to B6;SJL-Tg(ACTFLPe)9205Dym/J (Fig. 1A). Germline ablation of exon 26 from Cyt-$1^{fl/fl}$ mice was achieved by crossing neomycin-deleted offspring to EIIa-Cre mice and verified by PCR (Fig. 1B). ErbB4 Cyt-1 KOs are viable, have normal litter sizes (6.4 pups ± 0.11, N=2 cohorts; C57BL/6J 6.2 ± 0.2 pups (Nagasawa et al. 1973)) and exhibit no obvious anatomical, developmental or behavioral abnormalities. These observations were unexpected because germline deletion of ErbB4 results in embryonic lethality (Gassmann et al. 1995) and Cyt-1 transcripts account for 80% of all ErbB4 transcripts in heart (Veikkolainen et al. 2011; Chung et al. 2016; Erben et al. 2018), suggesting that ErbB4 Cyt-2 isoforms can functionally compensate for Cyt-1-containing receptors during cardiac development.

Using exon-specific primers and Taqman qRT-PCR, we quantified how removal of exon 26 affects the relative transcript levels of different ErbB4 Cyt-1/Cyt-2 and JMa/JMb receptor isoforms in brains of Cyt-1 heterozygote and KO mice (Fig. 1C). We found that Cyt-1 transcripts account for 40% of ErbB4 Cyt variants in whole brain RNA from controls, and that their levels are reduced to approximately half in Cyt-1 heterozygotes and undetectable in KOs (Fig. 1C, *left*). On the other hand, the relative levels of JMa to JMb receptor isoforms were similar across the three genotypes (Fig. 1C, *right*), indicating that splicing of ErbB4 transcripts at the two loci (JM and Cyt) are regulated independently. Importantly, removal of exon 26 and its splicing acceptor/donor sites did not affect overall receptor expression, as the total levels of ErbB4 transcripts relative to GAPDH in whole brain (Fig. 1D) are unchanged in Cyt-1 heterozygote and KO mice relative to controls, and only a small increase in ErbB4 transcripts was observed in the hippocampus of Cyt-1 KOs (Fig. 1E). Lastly, we investigated if expression of ErbB3 is affected in ErbB4 Cyt-1 KOs. This is important because Cyt-2 subunits could potentially heterodimerize with ErbB3 to activate downstream PI3K/Akt, as reported previously (Gambarotta et al. 2004), to compensate for loss of Cyt-1 isoforms. As expected, the relative levels of ErbB3 are lower than ErbB4, and we found that ErbB3 expression is unchanged in the whole brain (Fig. 1D) and hippocampus (Fig. 1E) of Cyt-1 heterozygote and KO mice relative to controls. Taken together, these results show that ErbB4 Cyt-1 KOs exclusively express Cyt-2 receptor isoforms that are not compensated by ErbB3.

Cyt-1 is expressed on cortical and hippocampal GABAergic interneurons, but dispensable for GABAergic interneuron development

ErbB4 Cyt-1 variants are highly expressed at ganglionic eminences and in migrating GABAergic neuroblasts during embryonic and postnatal development (Fornasari et al. 2016; Fregnan et al. 2014; Rakic et al. 2015), and adult ErbB4 KO mice have reduced cortical and hippocampal GABAergic interneurons (Flames et al. 2004; Neddens & Buonanno 2010). To test whether ErbB4 Cyt-1 is involved in the migration and/or maturation of GABAergic interneurons, using exon-specific ISH (i.e., BaseScope) we initially characterized the expression of Cyt-1 and Cyt-2 ErbB4 splice variants in the adult mouse dorsal hippocampus (Hpp) and somatosensory cortex (SSCtx). As shown in the representative micrographs, Cyt-1 (Fig. 2A) and Cyt-2 (Fig. 2B) isoforms were detected in a scattered pattern in the Hpp (*left*) and SSCtx (*right*), consistent with the distribution of GABAergic interneurons (Lai & Lemke 1991; Yau et al. 2003). Cyt-1 ErbB4 variants accounted for ~40% of total ErbB4 in both areas (Fig. 2C,D), similar to the relative levels previously reported (Neddens et al. 2011; Veikkolainen et al. 2011; Chung et al. 2016; Erben et al. 2018). These observations suggest that a significant portion of ErbB4 signaling in cortical and hippocampal GABAergic interneurons is mediated through ErbB4 Cyt-1 receptors.

Based on the aforementioned observations, we investigated if germline ablation of ErbB4 Cyt-1 receptors alters GABAergic interneuron migration by assessing interneuron numbers and distribution in the dorsal postnatal Hpp and SSCtx of WT, Cyt-1 heterozygote and Cyt-1 KO mice. For these experiments, GFP-labeled GABAergic interneurons were analyzed in mice derived from crosses between GAD-GFP transgenic (Tamamaki et al. 2003) and Cyt-1 KO mice (see Methods). Unexpectedly, GABAergic interneuron number was unchanged in the Hpp (Fig. 3A-C,G) and SSCtx (D-F,H) of young adult Cyt-1 heterozygote and KO

mice relative to controls (GAD-GFP cells in Hpp: Cyt-1 +/+ 180.8 ± 7.73 cells/mm^2, Cyt-1 +/− 178.1 ± 8.21 cells/mm^2, Cyt-1 −/− 180.1 ± 3.54 cells/mm^2; n=4, Kruskal-Wallis test, p=0.9410; in SSCtx: Cyt-1 +/+ 407.7 ± 10.71 cells/mm^2, Cyt-1 +/− 385.5 ± 7.10 cells/mm^2; Cyt-1 −/− 392.0 ± 11.99 cells/mm^2; n=4, one-way ANOVA F(2,9)=1.264, p=0.3283). Further analysis of the distribution of GAD-GFP expressing neurons in hippocampal areas CA1-CA3, dentate gyrus and subiculum (Fig. 3I), as well as layers I-VI of the SSCtx (Fig. 3J), failed to detect differences between WT and Cyt-1 heterozygote and KO mice. Based on these observations, we conclude that ErbB4 Cyt-1 isoforms are dispensable for GABAergic interneuron migration and postnatal viability.

Cyt-1 mutant mice exhibit minor behavioral abnormalities compared to ErbB4 null mice

ErbB4 null and conditional KO mice lacking ErbB4 selectively in PV+ interneurons (PV-Cre; ErbB4$^{fl/fl}$) exhibit numerous overlapping behavioral deficits, such as hyperactivity in the open field, reduced anxiety on the elevated plus maze and impaired PPI (Shamir et al. 2012; Skirzewski et al. 2020; Wen et al. 2010). To determine if ErbB4 Cyt-1 receptors contribute to these phenotypes, we subjected Cyt-1 KOs to a similar battery of behavioral tests (Fig. 4). We found that Cyt-1 heterozygote and KO mice traveled similar distances in the open field compared to their littermate WT controls, with a trend towards hypoactivity and faster habituation (Fig. 4A). In the elevated plus maze, Cyt-1 KOs and their controls spent similar time in the open and closed arms, suggesting that Cyt-1 KOs are not more anxious than controls (Fig. 4B). Next, we investigated sensory-motor responses of Cyt-1 mutants by measuring PPI to startle, a response that is altered in PV-Cre; ErbB4$^{fl/fl}$ and ErbB4 null mice and is an endophenotype associated with Scz. Initially, we measured startle responses to increasing intensities of sound and found that, although the overall startle responses were similar between controls, ErbB4 Cyt-1 heterozygote and KO mice (Fig. 4C, *left*), there was a significant interaction of sex and genotype in male (Fig. 4C, *center*: F(2,23)=5.321, p=0.0126*) but not female mice (Fig. 4C, *right*:, F(2,24)=0.01569, p=0.9844). We then proceeded to analyze PPI and observed no differences in sensorimotor gating between controls, ErbB4 Cyt-1 heterozygote and KO mice (Fig. 4D; two-way ANOVA, F(2,49)=0.1582, p=0.8541). These results suggest that ErbB4 Cyt-1 isoforms are unlikely to account for the behavioral phenotypes previously reported in ErbB4 null and PV-Cre; ErbB4$^{fl/fl}$ mice and that their functions can be compensated by Cyt-2 receptor isoforms.

Extracellular DA levels are augmented in ErbB4 Cyt-1 mutants

We (Skirzewski et al. 2018; Skirzewski et al. 2020) and others (Namba et al. 2016; Kato et al. 2011; Mizuno et al. 2013) previously reported that ErbB4 is expressed in approximately 90% of DAergic neurons in the mesencephalon, where it regulates the function of the DA reuptake transporter (Skirzewski et al. 2018; Skirzewski et al. 2020). Moreover, Th-Cre;ErbB4$^{fl/fl}$ mice exhibit an imbalance of extracellular DA levels in the mPFC that is rescued by microinjection of AAV-ErbB4 into the mesencephalon of adult Th-Cre;ErbB4$^{fl/fl}$ mice (Skirzewski et al. 2018; Skirzewski et al. 2020). To evaluate the role of Cyt-1 in modulating extracellular DA levels, we performed no-net-flux microdialysis in the mPFC of freely moving Cyt-1 KOs (Fig. 5A). Unexpectedly, we found that ErbB4 Cyt-1 heterozygote mice, but not Cyt-1 KOs, have increased basal extracellular DA levels (Fig. 5B; +/+ 0.546

± 0.080 nM, +/− 0.977 ± 0.103 nM, +/+ 0.689 ± 0.085 nM, n=6–7/genotype, one-way ANOVA, F(2,17)=5.863, *p=0.0116; +/+ vs. −/− p=0.4876, +/+ vs. +/− **p=0.0094, +/− vs. −/− p=0.089). The reasons for why ErbB4 Cyt-1 heterozygotes but not KOs exhibit differences in DA levels are presently unknown; potential reasons are discussed below (see Discussion).

ErbB4 Cyt-1 KOs and WT controls perform similarly on the Y- and Barnes-mazes

The alterations in extracellular DA levels in the mPFC of heterozygous Cyt-1 mice prompted us to investigate cognitive performance in mutant mice, which were previously reported to be impaired in ErbB4 null (Skirzewski et al. 2020; Wang et al. 2018; Tan et al. 2018) and Th-Cre;ErbB4$^{fl/fl}$ mice (Skirzewski et al. 2018). Mice were tested on a Y-maze spontaneous alternation task to assess spatial working memory, and in a Barnes maze to assess learning abilities and spatial reference memory. Novel arm preference in the Y-maze was unaltered in Cyt-1 KOs compared to controls (Fig. 6A). Next, we tested acquisition and recall of spatial reference memory in the Barnes maze. Cyt-1 KOs learned the task equally well compared to heterozygotes and controls, as evidenced by similar latency to escape (Fig. 6B) and number of errors committed during the 4-day training phase (Fig. 6C). Cyt-1 heterozygote and KO mice performed similarly to controls in the probe test that measures the number of errors, time spent in the correct zone and the number of nose pokes/hole, including the target escape hole (Fig. 6D-F). Finally, we tested cognitive flexibility and perseverance by moving the escape target in the Barnes maze to a new location. All three genotypes adapted equally to the new paradigm as indicated by similar latencies to escape (Fig. 6G) and errors committed during the four trials (Fig. 6H). Taken together, these findings show that germline deletion of ErbB4 Cyt-1 isoforms does not affect cognitive behaviors previously shown to be altered in ErbB4 null and targeted Th-Cre;ErbB4$^{fl/fl}$ mice, and they suggest that the functions of ErbB4 Cyt-1 receptors are potentially compensated during development by Cyt-2 isoforms.

Behavioral effects are observed when ErbB4 Cyt-1 is acutely targeted in the adult VTA

To circumvent possible developmental compensation in germline ErbB4 Cyt-1 KOs, we employed an *acute* loss-of-function paradigm in adulthood by injecting AAV-Cre into the VTA of ErbB4 Cyt-1$^{fl/fl}$ mice (Fig. 7A). Because direct detection of Cyt-1 recombination is technically challenging, we injected control littermate mice with AAV9-hSynI-GFP and acutely targeted the floxed Cyt-1 exon in ErbB4 Cyt-1$^{fl/fl}$ mice (hereafter referred as “acute Cyt-1 KOs”) by co-injecting AAV9-hSynI-Cre and AAV9-hSynI-DIO-GFP. Cre-mediated recombination was effective in mesencephalic DAergic neurons, as judged by the presence of numerous TH-positive neurons that co-label with GFP (Fig. S2). Importantly, we used low AAV-Cre titers that were sufficiently high to recombine *loxP* sites but that did not alter the expression of TH or DAT non-specifically as others (Rezai Amin et al. 2019) and we (unpublished) observed when using higher AAV-Cre titers (DAT ctrl vs. Cre p=0.7531; TH ctrl vs. Cre p=0.7471, n=8–11/group, Welch’s test).

After allowing time for recovery and recombination (see Methods), cohorts of acute Cyt-1 KOs and controls were tested on different behavioral tasks. In the elevated plus maze, acute Cyt-1 KOs spent less time in the closed arms compared to controls (Fig. 7B;

two-way ANOVA, F(1,17)=4.421, p=0.0507, Sidak's multiple comparison test controls vs. Cyt-1 KOs p=0.0234*), suggesting reduced anxiety levels in acute Cyt-1 KOs. Next, we used Y-maze spontaneous alternation to evaluate hippocampal and mPFC function because we recently reported that re-expression of ErbB4 in the VTA of adult Th-Cre; ErbB4$^{fl/fl}$ mice restores their performance in this task (Skirzewski et al. 2018). We found that alternation in the Y-maze, which evaluates working memory, did not differ between acute Cyt-1 KOs and controls (Fig. 7C). Lastly, the two cohorts of mice were tested for the acoustic startle response and PPI. Interestingly, acute Cyt-1 KOs showed increased startle responses relative to controls (Fig. 7D; mixed-effects analysis, F(11,181)=1.874, p=0.454*, ctrl vs. Cre p=0.0490*), but PPI was unaffected (Fig. 7E; two-way ANOVA, F(3,51)=0.09446, p=0.9628, ctrl vs. Cre p=0.0601). When the results of acute exon 26 ablation are taken together with the effects on DA levels and behaviors we observed in ErbB4 Cyt-1 heterozygote mice, they suggest that Cyt-2 receptor isoforms can effectively compensate for the lack of Cyt-1 isoforms during development and to a lesser extent when deleted acutely in adults (see Discussion).

Discussion

We were interested in studying the effects of germline and acute ablation of the ErbB4 Cyt-1 receptor isoform in adults because numerous studies have underscored the importance of ErbB4 function during development and continued expression in mature mice for regulating DA levels, neuronal plasticity and behaviors (Del Pino et al. 2013; Shamir et al. 2012; Skirzewski et al. 2018; Wang et al. 2018; Wen et al. 2010). Moreover, polymorphisms regulating Cyt-1 splicing (Law et al. 2007; Silberberg et al. 2006) and Cyt-1/Cyt-2 transcript ratios in the postmortem DLPFC of patients are both associated with risk for Scz (Chung et al. 2016; Joshi et al. 2014; Law et al. 2007; Silberberg et al. 2006). We undertook the present studies to investigate the functional role of ErbB4 Cyt-1 receptors *in vivo*, by generating a novel conditional Cyt-1$^{fl/fl}$ mouse line used to excise exon 26 either constitutively in the germline or acutely in the adult brain by microinjecting AAV-Cre in the VTA.

Developmental loss of ErbB4 Cyt-1 receptors in germline KOs is partially compensated

Although Cyt-1 is the major cardiac ErbB4 isoform (~80 %), we unexpectedly found that germline Cyt-1 KOs are viable. Similarly, although Cyt-1 comprises ~40% of the receptor in the brain, germline ablation of Cyt-1 receptors does not result in a loss of GABAergic interneurons during neurodevelopment, as had been previously observed in ErbB4 null mice (Perez-Garcia 2015; Li et al. 2012), and Cyt-1 KOs exhibit minor behavioral impairments relative to ErbB4 KOs (Fazzari et al. 2010; Flames et al. 2004; Shamir et al. 2012; Skirzewski et al. 2018). Nevertheless, we observed that heterozygote Cyt-1 mutants exhibit elevated basal extracellular DA levels in the mPFC (Fig. 5), suggesting that mutation of both ErbB4 exon 26 alleles may be required to trigger alternative mechanisms to compensate for loss of Cyt-1-mediated PI3K/Akt signaling during cardiac and neuronal development.

While it is unlikely that Cyt-1 and Cyt-2 ErbB4 receptors exert completely redundant functions *in vivo*, given that expression of both isoforms has been conserved through evolution, our data strongly suggests that loss of Cyt-1 can be compensated on a cellular

or systemic level in both the heart and the brain. Of note, total ErbB4 transcript levels are unchanged in Cyt-1 KO mice and, instead, removal of exon 26 directs all splicing to generate exclusively the Cyt-2 isoform (Fig. 1C,D). The loss of Cyt-1-containing receptors could arguably be compensated functionally by the heterodimerization of ErbB4 Cyt-2 with ErbB3 receptors to indirectly activate PI3K (Elenius et al. 1999; Gambarotta et al. 2004). However, this possibility seems remote for the following reasons: 1) ErbB3 mRNA expression is generally undetectable in the developing heart and in central neurons (Steiner et al. 1999; Pinkas-Kramarski et al. 1997), 2) ErbB3 expression does not increase in the brain of Cyt1 KOs (Fig. 1E) and 3) ErbB4 functions were not compensated in mice harboring germline mutations of the receptor (Shamir et al. 2012) or in conditional mice with targeted ErbB4 ablation in either GABAergic (Flames et al. 2004; Fazzari et al. 2010; Shamir et al. 2012; Skirzewski et al. 2018; Mei & Nave 2014) or DAergic (Skirzewski et al. 2018) neurons, indicating that continued ErbB4 function is required in the adult and cannot be compensated by ErbB3. Other potential compensatory mechanisms are that MAPK signaling downstream of ErbB4 Cyt-2 positively regulates PI3K/Akt/mTOR, as previously reported (Mendoza et al. 2011), or that it is the structural roles of the receptor, rather than its kinase activity, that regulate many of the functions attributed to ErbB4. For example, NRG modulates the expression of GABA alpha1 receptors in an ErbB4-dependent, but kinase-independent mode (Mitchell et al. 2013), and NRG3 regulates ErbB4-containing glutamatergic synapses on GABAergic interneurons without activating ErbB4 kinase activity (Muller et al. 2018). Hence, several of the behavioral abnormalities observed in ErbB4 KOs could have resulted from the physical loss of the receptor and not its kinase and downstream signaling activities.

Some functions of Cyt-1 isoforms are not compensated when acutely targeted in adult mice

The deficits in neurotransmission, neuronal plasticity and behaviors observed in mice that develop in the absence of ErbB4 (Del Pino et al. 2013; Shamir et al. 2012; Skirzewski et al. 2018; Wang et al. 2018; Wen et al. 2010) can be rescued in adult mice by re-expressing ErbB4 (Wang et al. 2018; Skirzewski et al. 2018) or pharmacologically reactivating (Wang et al. 2018; Skirzewski et al. 2018) receptor function, indicating a continued requirement for ErbB4 in the adult. Interestingly, we found that these findings are consistent with our experiments using acute ablation of Cyt-1 receptors in the mouse VTA that resulted in increased startle responses and reduced time in the closed arms of an elevated plus maze, which was not observed in germline ErbB4 Cyt-1 KOs, thus uncovering functions for these receptor variants in adult mice that cannot be compensated by ErbB4 Cyt-2 isoforms.

Potential importance of ErbB4 Cyt isoforms in schizophrenia

Polymorphisms in *ERBB4* have been linked to an increased risk for Scz. While the question of whether total ErbB4 levels are unchanged or increased in Scz is controversial (see (Chung et al. 2016; Joshi et al. 2014)), five independent studies have identified an increased ratio of JMa and Cyt-1 to JMb and Cyt-2 transcript levels in the DLPFC of Scz patients (Silberberg et al. 2006; Law et al. 2007; Law et al. 2012; Joshi et al. 2014; Chung et al. 2016; Chung et al. 2018). The increased ratio of JMa/Cyt-1 to JMb/Cyt-2 transcripts is associated with a selective decrease of synaptic inputs and parvalbumin expression, indicative of

reduced function, in postmortem DLPFC GABAergic interneurons of persons diagnosed with Scz and mood disorders (Chung et al. 2018; Chung et al. 2016). Moreover, ErbB4 polymorphisms were shown to correlate with increased Cyt-1 and PI3KCD expression (Law et al. 2007; Law et al. 2012; Silberberg et al. 2006), and a link between Cyt-1 and PI3K/Akt signaling has been viewed as a potentially novel target for the treatment of Scz (Law et al. 2007; Law et al. 2012). Until this work, no study to date has directly targeted Cyt splice variants to investigate their functional roles *in vivo*. Our findings demonstrate that downstream PI3K/Akt functions mediated by ErbB4 Cyt-1 receptors can be partially compensated by Cyt-2 receptor isoforms in inbred captive mice, particularly in GABAergic interneurons. Although it is presently unknown if ErbB4 Cyt-1 functions in distinct environmental situations or in different species can be compensated by ErbB4 Cyt-2 isoforms to the same extent, the ErbB4 $Cyt1^{f/f}$ mouse line provides a novel tool to test the specificity of drugs that target the coupling between Cyt-1 and the PI3K/Akt signaling pathway and represent a potentially novel therapeutic strategy for the treatment of Scz (Law et al. 2007; Law et al. 2012). This study represents an important initial step for understanding the distinct and unique functions of different ErbB4 receptor isoforms *in vivo*. Given the consistent findings showing that the relative ratios of ErbB4 JMa/JMb and Cyt-1/Cyt-2 splice variants are affected in Scz (Silberberg et al. 2006; Law et al. 2007; Law et al. 2012; Joshi et al. 2014; Chung et al. 2016) and mood disorders (Chung et al. 2018), in the future it will be important to continue assessing the effects of ErbB4 Cyt-1 receptor loss- and gain-of-function in other neuronal subtypes, as well as the specific functions attributable to either JMa or JMb receptor subtypes.

Supplementary Material

Refer to Web version on PubMed Central for supplementary material.

Acknowledgements

The authors thank Dr. Carolyn Smith from the Light Imaging Facility (NINDS) and Dr. Vincent Schram from the Microscopy and Imaging Core (NICHD) for support with fluorescence microscopy. We thank Drs. Steven Coon and James Iben at the Molecular Genomics Core (NICHD) for help with RNA sequencing, and Dr. Yuchio Yanagawa at Gunma University, Japan for the GAD67-GFP mice. We are grateful to Daniel Abebe for help with animal care and to Arihant Chadda for help with initial PCR studies. This work was supported by the Intramural Research Program of the Eunice Kennedy Shriver National Institute of Child Health and Human Development (NICHD; ZIA-HD000711 to A.B.) and by the Department of Defense (CDMRP; W81XWH-12-1-0164 to S.L.C.).

Abbreviations:

AAV	adeno-associated virus
aCSF	artificial cerebral spinal fluid
CNS	central nervous system
Cyt	cytoplasmic
Cyt-1 KOs	Cyt-1 knockout mice
DA	dopamine/dopaminergic

DAT	dopamine transporter
Dbh	dopamine beta-hydroxylase
DLPFC	dorsal lateral prefrontal cortex
ErbB4 KOs	heart-rescued ErbB4 knockout mice
ES	embryonic stem
GFP	green-fluorescent protein
HPLC	high performance liquid chromatography
Hpp	hippocampus
IHC	immunofluorescence histochemistry
ISH	in-situ hybridization
JM	juxtamembrane
KO	knockout
mPFC	medial prefrontal cortex
NPP	no pre-pulse
NRGs	neuregulins
P13K	phosphatidylinositol-3-kinase
PBS	phosphate-buffered saline
PFA	paraformaldehyde
PPI	pre-pulse inhibition
PPXY	WW domain motif
PV	parvalbumin
RRIDs	Research Resource Identifier (see scicrunch.org)
RT-qPCR	reverse-transcription polymerase chain reaction
Scz	Schizophrenia
SSCtx	somatosensory cortex
TH	tyrosine hydroxylase
VTA	ventral tegmental area

References:

Abe Y, Namba H, Zheng Y. and Nawa H. (2009) In situ hybridization reveals developmental regulation of ErbB1–4 mRNA expression in mouse midbrain: implication of ErbB receptors for dopaminergic neurons. Neuroscience 161, 95–110. [PubMed: 19298847]

Andersson RH, Johnston A, Herman PA, Winzer-Serhan UH, Karavanova I, Vullhorst D, Fisahn A. and Buonanno A. (2012) Neuregulin and dopamine modulation of hippocampal gamma oscillations is dependent on dopamine D4 receptors. Proc Natl Acad Sci U S A 109, 13118–13123. [PubMed: 22822214]

Bartolini G, Sanchez-Alcaniz JA, Osorio C, Valiente M, Garcia-Frigola C. and Marin O. (2017) Neuregulin 3 Mediates Cortical Plate Invasion and Laminar Allocation of GABAergic Interneurons. Cell Rep 18, 1157–1170. [PubMed: 28147272]

Buonanno A. (2010) The neuregulin signaling pathway and schizophrenia: from genes to synapses and neural circuits. Brain Res Bull 83, 122–131. [PubMed: 20688137]

Buonanno A. and Fischbach GD (2001) Neuregulin and ErbB receptor signaling pathways in the nervous system. Curr Opin Neurobiol 11, 287–296. [PubMed: 11399426]

Carpenter AE, Jones TR, Lamprecht MR et al. (2006) CellProfiler: image analysis software for identifying and quantifying cell phenotypes. Genome Biol 7, R100. [PubMed: 17076895]

Chen YJ, Zhang M, Yin DM et al. (2010) ErbB4 in parvalbumin-positive interneurons is critical for neuregulin 1 regulation of long-term potentiation. Proc Natl Acad Sci U S A 107, 21818–21823.

Chung DW, Chung Y, Bazmi HH and Lewis DA (2018) Altered ErbB4 splicing and cortical parvalbumin interneuron dysfunction in schizophrenia and mood disorders. Neuropsychopharmacology 43, 2478–2486. [PubMed: 30120408]

Chung DW, Volk DW, Arion D, Zhang Y, Sampson AR and Lewis DA (2016) Dysregulated ErbB4 Splicing in Schizophrenia: Selective Effects on Parvalbumin Expression. Am J Psychiatry 173, 60–68. [PubMed: 26337038]

Del Pino I, Garcia-Frigola C, Dehorter N. et al. (2013) Erbb4 deletion from fast-spiking interneurons causes schizophrenia-like phenotypes. Neuron 79, 1152–1168. [PubMed: 24050403]

Elenius K, Choi CJ, Paul S, Santiestevan E, Nishi E. and Klagsbrun M. (1999) Characterization of a naturally occurring ErbB4 isoform that does not bind or activate phosphatidyl inositol 3-kinase. Oncogene 18, 2607–2615. [PubMed: 10353604]

Elenius K, Corfas G, Paul S, Choi CJ, Rio C, Plowman GD and Klagsbrun M. (1997) A novel juxtamembrane domain isoform of HER4/ErbB4. Isoform-specific tissue distribution and differential processing in response to phorbol ester. J Biol Chem 272, 26761–26768.

Erben L. and Buonanno A. (2019) Detection and Quantification of Multiple RNA Sequences Using Emerging Ultrasensitive Fluorescent In Situ Hybridization Techniques. Curr Protoc Neurosci, e63. [PubMed: 30791216]

Erben L, He MX, Laeremans A, Park E. and Buonanno A. (2018) A Novel Ultrasensitive In Situ Hybridization Approach to Detect Short Sequences and Splice Variants with Cellular Resolution. Mol Neurobiol 55, 6169–6181. [PubMed: 29264769]

Fazzari P, Paternain AV, Valiente M, Pla R, Lujan R, Lloyd K, Lerma J, Marin O. and Rico B. (2010) Control of cortical GABA circuitry development by Nrg1 and ErbB4 signalling. Nature 464, 1376–1380. [PubMed: 20393464]

Fisahn A, Neddens J, Yan L. and Buonanno A. (2009) Neuregulin-1 modulates hippocampal gamma oscillations: implications for schizophrenia. Cereb Cortex 19, 612–618. [PubMed: 18632742]

Flames N, Long JE, Garratt AN, Fischer TM, Gassmann M, Birchmeier C, Lai C, Rubenstein JL and Marin O. (2004) Short- and long-range attraction of cortical GABAergic interneurons by neuregulin-1. Neuron 44, 251–261. [PubMed: 15473965]

Fornasari BE, El Soury M, De Marchis S, Perroteau I, Geuna S. and Gambarotta G. (2016) Neuregulin1 alpha activates migration of neuronal progenitors expressing ErbB4. Mol Cell Neurosci 77, 87–94. [PubMed: 27989735]

Fregnan F, Gnavi S, Macri L, Perroteau I. and Gambarotta G. (2014) The four isoforms of the tyrosine kinase receptor ErbB4 provide neural progenitor cells with an adhesion preference for the

transmembrane type III isoform of the ligand neuregulin 1. Neuroreport 25, 233–241. [PubMed: 24518229]

Fregnan F, Petrov V, Garzotto D, De Marchis S, Offenhauser N, Grosso E, Chiorino G, Perroteau I. and Gambarotta G. (2011) Eps8 involvement in neuregulin1-ErbB4 mediated migration in the neuronal progenitor cell line ST14A. Exp Cell Res 317, 757–769. [PubMed: 21281626]

Friend DM, Devarakonda K, O'Neal TJ et al. (2017) Basal Ganglia Dysfunction Contributes to Physical Inactivity in Obesity. Cell Metab 25, 312–321. [PubMed: 28041956]

Gambarotta G, Garzotto D, Destro E. et al. (2004) ErbB4 expression in neural progenitor cells (ST14A) is necessary to mediate neuregulin-1beta1-induced migration. J Biol Chem 279, 48808–48816.

Gassmann M, Casagranda F, Orioli D, Simon H, Lai C, Klein R. and Lemke G. (1995) Aberrant neural and cardiac development in mice lacking the ErbB4 neuregulin receptor. Nature 378, 390–394. [PubMed: 7477376]

Greenwood TA, Light GA, Swerdlow NR, Radant AD and Braff DL (2012) Association analysis of 94 candidate genes and schizophrenia-related endophenotypes. PLoS One 7, e29630.

Gu Y, Tran T, Murase S, Borrell A, Kirkwood A. and Quinlan EM (2016) Neuregulin-Dependent Regulation of Fast-Spiking Interneuron Excitability Controls the Timing of the Critical Period. J Neurosci 36, 10285–10295.

Hayes LN, Shevelkin A, Zeledon M. et al. (2016) Neuregulin 3 Knockout Mice Exhibit Behaviors Consistent with Psychotic Disorders. Mol Neuropsychiatry 2, 79–87. [PubMed: 27606322]

Heredia-Lopez FJ, Alvarez-Cervera FJ, Colli-Alfaro JG, Bata-Garcia JL, Arankowsky-Sandoval G. and Gongora-Alfaro JL (2016) An automated Y-maze based on a reduced instruction set computer (RISC) microcontroller for the assessment of continuous spontaneous alternation in rats. Behav Res Methods 48, 1631–1643. [PubMed: 26563396]

Hernandez L, Stanley BG and Hoebel BG (1986) A small, removable microdialysis probe. Life Sci 39, 2629–2637. [PubMed: 2432375]

Joshi D, Fullerton JM and Weickert CS (2014) Elevated ErbB4 mRNA is related to interneuron deficit in prefrontal cortex in schizophrenia. J Psychiatr Res 53, 125–132. [PubMed: 24636039]

Kainulainen V, Sundvall M, Maatta JA, Santiestevan E, Klagsbrun M. and Elenius K. (2000) A natural ErbB4 isoform that does not activate phosphoinositide 3-kinase mediates proliferation but not survival or chemotaxis. J Biol Chem 275, 8641–8649. [PubMed: 10722704]

Kato T, Abe Y, Sotoyama H, Kakita A, Kominami R, Hirokawa S, Ozaki M, Takahashi H. and Nawa H. (2011) Transient exposure of neonatal mice to neuregulin-1 results in hyperdopaminergic states in adulthood: implication in neurodevelopmental hypothesis for schizophrenia. Mol Psychiatry 16, 307–320. [PubMed: 20142818]

Kim J. and Shin W. (2014) How to do random allocation (randomization). Clin Orthop Surg 6, 103–109. [PubMed: 24605197]

Kotzadimitriou D, Nissen W, Paizs M, Newton K, Harrison PJ, Paulsen O. and Lamsa K. (2018) Neuregulin 1 Type I Overexpression Is Associated with Reduced NMDA Receptor-Mediated Synaptic Signaling in Hippocampal Interneurons Expressing PV or CCK. eNeuro 5.

Kwon OB, Paredes D, Gonzalez CM, Neddens J, Hernandez L, Vullhorst D. and Buonanno A. (2008) Neuregulin-1 regulates LTP at CA1 hippocampal synapses through activation of dopamine D4 receptors. Proc Natl Acad Sci U S A 105, 15587–15592.

Lai C. and Lemke G. (1991) An extended family of protein-tyrosine kinase genes differentially expressed in the vertebrate nervous system. Neuron 6, 691–704. [PubMed: 2025425]

Law AJ, Kleinman JE, Weinberger DR and Weickert CS (2007) Disease-associated intronic variants in the ErbB4 gene are related to altered ErbB4 splice-variant expression in the brain in schizophrenia. Hum Mol Genet 16, 129–141. [PubMed: 17164265]

Law AJ, Wang Y, Sei Y. et al. (2012) Neuregulin 1-ErbB4-PI3K signaling in schizophrenia and phosphoinositide 3-kinase-p110delta inhibition as a potential therapeutic strategy. Proc Natl Acad Sci U S A 109, 12165–12170.

Li H, Chou SJ, Hamasaki T, Perez-Garcia CG and O'Leary DD (2012) Neuregulin repellent signaling via ErbB4 restricts GABAergic interneurons to migratory paths from ganglionic eminence to cortical destinations. Neural Dev 7, 10. [PubMed: 22376909]

Li K, Turner AN, Chen M. et al. (2016) Mice with missense and nonsense NF1 mutations display divergent phenotypes compared with human neurofibromatosis type I. Dis Model Mech 9, 759–767. [PubMed: 27482814]

Liu P, Jenkins NA and Copeland NG (2003) A highly efficient recombineering-based method for generating conditional knockout mutations. Genome Res 13, 476–484. [PubMed: 12618378]

Lu Y, Sun XD, Hou FQ et al. (2014) Maintenance of GABAergic activity by neuregulin 1-ErbB4 in amygdala for fear memory. Neuron 84, 835–846. [PubMed: 25451196]

Mei L. and Nave KA (2014) Neuregulin-ERBB signaling in the nervous system and neuropsychiatric diseases. Neuron 83, 27–49. [PubMed: 24991953]

Mendoza MC, Er EE and Blenis J. (2011) The Ras-ERK and PI3K-mTOR pathways: cross-talk and compensation. Trends Biochem Sci 36, 320–328. [PubMed: 21531565]

Mitchell RM, Janssen MJ, Karavanova I, Vullhorst D, Furth K, Makusky A, Markey SP and Buonanno A. (2013) ErbB4 reduces synaptic GABAA currents independent of its receptor tyrosine kinase activity. Proc Natl Acad Sci U S A 110, 19603–19608.

Mizuno M, Sotoyama H, Namba H. et al. (2013) ErbB inhibitors ameliorate behavioral impairments of an animal model for schizophrenia: implication of their dopamine-modulatory actions. Transl Psychiatry 3, e252. [PubMed: 23632456]

Mostaid MS, Lloyd D, Liberg B. et al. (2016) Neuregulin-1 and schizophrenia in the genome-wide association study era. Neurosci Biobehav Rev 68, 387–409. [PubMed: 27283360]

Muller T, Braud S, Juttner R. et al. (2018) Neuregulin 3 promotes excitatory synapse formation on hippocampal interneurons. EMBO J 37.

Nagasawa H, Miyamoto M. and Fujimoto M. (1973) [Reproductivity in inbred strains of mice and project for their efficient production (author's transl)]. Jikken Dobutsu 22, 119–126. [PubMed: 4796585]

Namba H, Okubo T. and Nawa H. (2016) Perinatal Exposure to Neuregulin-1 Results in Disinhibition of Adult Midbrain Dopaminergic Neurons: Implication in Schizophrenia Modeling. Sci Rep 6, 22606.

Nason MW Jr., Adhikari A, Bozinoski M, Gordon JA and Role LW (2011) Disrupted activity in the hippocampal-accumbens circuit of type III neuregulin 1 mutant mice. Neuropsychopharmacology 36, 488–496. [PubMed: 20927045]

Neddens J. and Buonanno A. (2010) Selective populations of hippocampal interneurons express ErbB4 and their number and distribution is altered in ErbB4 knockout mice. Hippocampus 20, 724–744. [PubMed: 19655320]

Neddens J, Fish KN, Tricoire L, Vullhorst D, Shamir A, Chung W, Lewis DA, McBain CJ and Buonanno A. (2011) Conserved interneuron-specific ErbB4 expression in frontal cortex of rodents, monkeys, and humans: implications for schizophrenia. Biol Psychiatry 70, 636–645. [PubMed: 21664604]

Omerovic J, Puggioni EM, Napoletano S, Visco V, Fraioli R, Frati L, Gulino A. and Alimandi M. (2004) Ligand-regulated association of ErbB-4 to the transcriptional co-activator YAP65 controls transcription at the nuclear level. Exp Cell Res 294, 469–479. [PubMed: 15023535]

Perez-Garcia CG (2015) ErbB4 in Laminated Brain Structures: A Neurodevelopmental Approach to Schizophrenia. Front Cell Neurosci 9, 472. [PubMed: 26733804]

Pinkas-Kramarski R, Eilam R, Alroy I, Levkowitz G, Lonai P. and Yarden Y. (1997) Differential expression of NDF/neuregulin receptors ErbB-3 and ErbB-4 and involvement in inhibition of neuronal differentiation. Oncogene 15, 2803–2815. [PubMed: 9419971]

Rakic S, Kanatani S, Hunt D. et al. (2015) Cdk5 phosphorylation of ErbB4 is required for tangential migration of cortical interneurons. Cereb Cortex 25, 991–1003. [PubMed: 24142862]

Rezai Amin S, Gruszczynski C, Guiard BP, Callebert J, Launay JM, Louis F, Betancur C, Vialou V. and Gautron S. (2019) Viral vector-mediated Cre recombinase expression in substantia nigra induces lesions of the nigrostriatal pathway associated with perturbations of dopamine-related behaviors and hallmarks of programmed cell death. J Neurochem 150, 330–340. [PubMed: 30748001]

Shamir A, Kwon OB, Karavanova I, Vullhorst D, Leiva-Salcedo E, Janssen MJ and Buonanno A. (2012) The importance of the NRG-1/ErbB4 pathway for synaptic plasticity and behaviors associated with psychiatric disorders. J Neurosci 32, 2988–2997. [PubMed: 22378872]

Silberberg G, Darvasi A, Pinkas-Kramarski R. and Navon R. (2006) The involvement of ErbB4 with schizophrenia: association and expression studies. Am J Med Genet B Neuropsychiatr Genet 141B, 142–148. [PubMed: 16402353]

Skirzewski M, Cronin ME, Murphy R, Fobbs W, Kravitz AV and Buonanno A. (2020) ErbB4 Null Mice Display Altered Mesocorticolimbic and Nigrostriatal Dopamine Levels as well as Deficits in Cognitive and Motivational Behaviors. eNeuro 7.

Skirzewski M, Karavanova I, Shamir A. et al. (2018) ErbB4 signaling in dopaminergic axonal projections increases extracellular dopamine levels and regulates spatial/working memory behaviors. Mol Psychiatry 23, 2227–2237. [PubMed: 28727685]

Slifstein M, van de Giessen E, Van Snellenberg J. et al. (2015) Deficits in prefrontal cortical and extrastriatal dopamine release in schizophrenia: a positron emission tomographic functional magnetic resonance imaging study. JAMA Psychiatry 72, 316–324. [PubMed: 25651194]

Stefansson H, Sigurdsson E, Steinthorsdottir V. et al. (2002) Neuregulin 1 and susceptibility to schizophrenia. Am J Hum Genet 71, 877–892. [PubMed: 12145742]

Steiner H, Blum M, Kitai ST and Fedi P. (1999) Differential expression of ErbB3 and ErbB4 neuregulin receptors in dopamine neurons and forebrain areas of the adult rat. Exp Neurol 159, 494–503. [PubMed: 10506520]

Sun Y, Ikrar T, Davis MF et al. (2016) Neuregulin-1/ErbB4 Signaling Regulates Visual Cortical Plasticity. Neuron 92, 160–173. [PubMed: 27641496]

Tamamaki N, Yanagawa Y, Tomioka R, Miyazaki J, Obata K. and Kaneko T. (2003) Green fluorescent protein expression and colocalization with calretinin, parvalbumin, and somatostatin in the GAD67-GFP knock-in mouse. J Comp Neurol 467, 60–79. [PubMed: 14574680]

Tan Z, Robinson HL, Yin DM et al. (2018) Dynamic ErbB4 Activity in Hippocampal-Prefrontal Synchrony and Top-Down Attention in Rodents. Neuron 98, 380–393 e384. [PubMed: 29628188]

Tidcombe H, Jackson-Fisher A, Mathers K, Stern DF, Gassmann M. and Golding JP (2003) Neural and mammary gland defects in ErbB4 knockout mice genetically rescued from embryonic lethality. Proc Natl Acad Sci U S A 100, 8281–8286. [PubMed: 12824469]

Veikkolainen V, Vaparanta K, Halkilahti K, Iljin K, Sundvall M. and Elenius K. (2011) Function of ERBB4 is determined by alternative splicing. Cell Cycle 10, 2647–2657. [PubMed: 21811097]

Vullhorst D, Ahmad T, Karavanova I, Keating C. and Buonanno A. (2017) Structural Similarities between Neuregulin 1–3 Isoforms Determine Their Subcellular Distribution and Signaling Mode in Central Neurons. J Neurosci 37, 5232–5249. [PubMed: 28432142]

Vullhorst D, Mitchell RM, Keating C, Roychowdhury S, Karavanova I, Tao-Cheng JH and Buonanno A. (2015) A negative feedback loop controls NMDA receptor function in cortical interneurons via neuregulin 2/ErbB4 signalling. Nat Commun 6, 7222. [PubMed: 26027736]

Vullhorst D, Neddens J, Karavanova I, Tricoire L, Petralia RS, McBain CJ and Buonanno A. (2009) Selective expression of ErbB4 in interneurons, but not pyramidal cells, of the rodent hippocampus. J Neurosci 29, 12255–12264.

Wang H, Liu F, Chen W. et al. (2018) Genetic recovery of ErbB4 in adulthood partially restores brain functions in null mice. Proc Natl Acad Sci U S A 115, 13105–13110.

Weinstein JJ, Chohan MO, Slifstein M, Kegeles LS, Moore H. and Abi-Dargham A. (2017) Pathway-Specific Dopamine Abnormalities in Schizophrenia. Biol Psychiatry 81, 31–42. [PubMed: 27206569]

Wen L, Lu YS, Zhu XH et al. (2010) Neuregulin 1 regulates pyramidal neuron activity via ErbB4 in parvalbumin-positive interneurons. Proc Natl Acad Sci U S A 107, 1211–1216. [PubMed: 20080551]

Woo RS, Li XM, Tao Y. et al. (2007) Neuregulin-1 enhances depolarization-induced GABA release. Neuron 54, 599–610. [PubMed: 17521572]

Yan L, Shamir A, Skirzewski M. et al. (2018) Neuregulin-2 ablation results in dopamine dysregulation and severe behavioral phenotypes relevant to psychiatric disorders. Mol Psychiatry 23, 1233–1243. [PubMed: 28322273]

Yang JM, Shen CJ, Chen XJ, Kong Y, Liu YS, Li XW, Chen Z, Gao TM and Li XM (2018) erbb4 Deficits in Chandelier Cells of the Medial Prefrontal Cortex Confer Cognitive Dysfunctions: Implications for Schizophrenia. Cereb Cortex.

Yang JM, Zhang J, Chen XJ, Geng HY, Ye M, Spitzer NC, Luo JH, Duan SM and Li XM (2013) Development of GABA circuitry of fast-spiking basket interneurons in the medial prefrontal cortex of erbb4-mutant mice. J Neurosci 33, 19724–19733.

Yau HJ, Wang HF, Lai C. and Liu FC (2003) Neural development of the neuregulin receptor ErbB4 in the cerebral cortex and the hippocampus: preferential expression by interneurons tangentially migrating from the ganglionic eminences. Cereb Cortex 13, 252–264. [PubMed: 12571115]

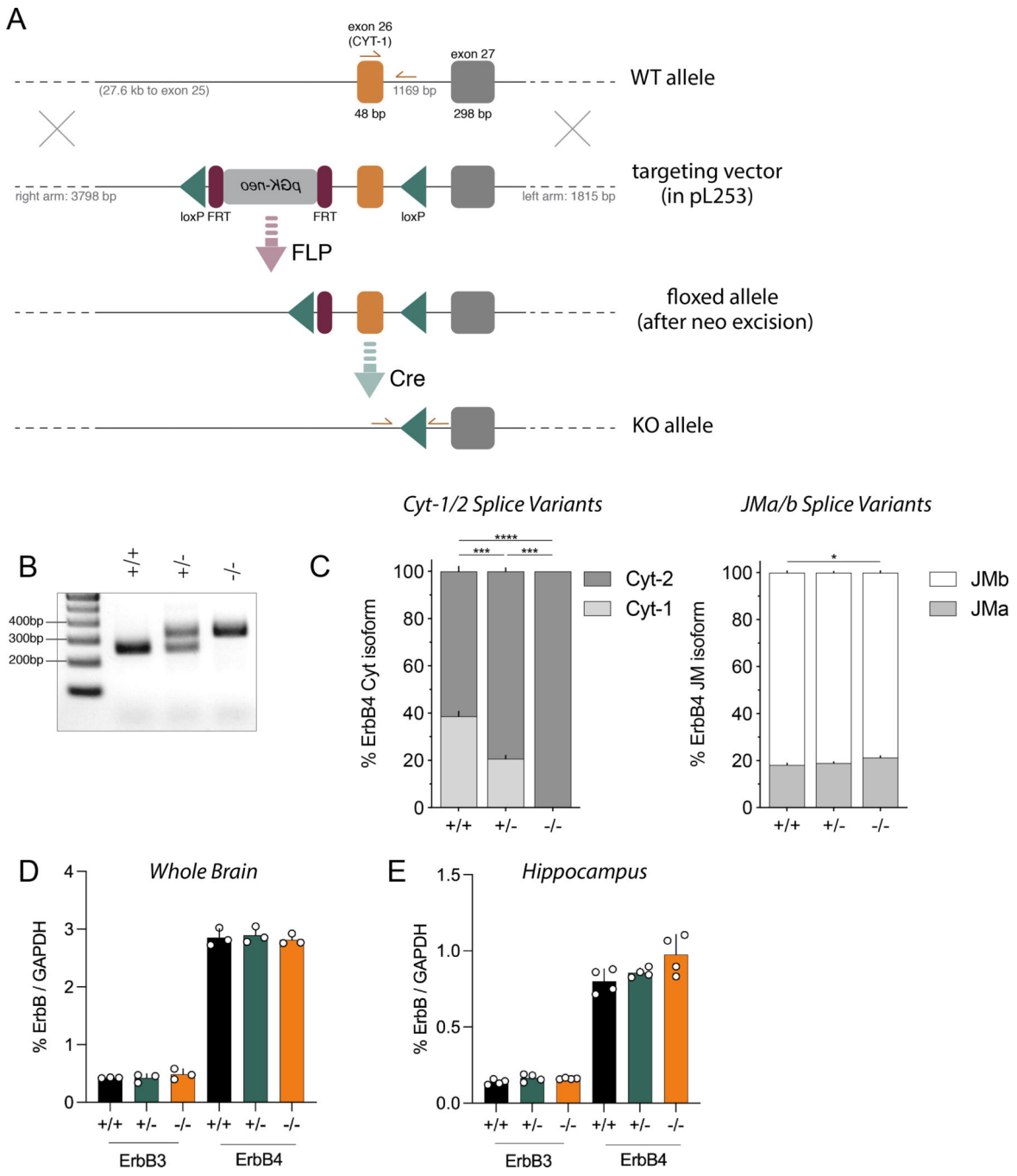

Figure 1. Generation of ErbB4 Cyt-1 KO mice and analysis of receptor splice variants.

A) Targeting strategy to generate Cyt-1 mutant mice (for more details see Methods). Exon 26 (*orange*), encoding the Cyt-1 cassette, was targeted by site-specific recombination in C57BL/6J-derived embryonic stem cells to insert flanking loxP sites (*green*). Subsequently, the FRT-pGK-neo-FRT selection cassette (*magenta*) was removed in mice harboring the targeted allele by crossing to a FLP deleter strain. The Cyt-1 exon was then ablated in ablated in germline by crossing to mice expressing Cre recombinase under control of the ubiquitously active EIIa promoter. ***B***) Representative genotyping results using primers

indicated in *panel A*. ***C***) Relative levels of different ErbB4 splice variants in whole brain RNA quantified by Taqman qRT-PCR using specific primers for either Cyt-1/Cyt-2 (*left*) or JMa/JMb (*right*) isoforms (n=3/genotype). Cyt-1 transcripts were undetectable in Cyt-1 KOs and reduced by approximately half in heterozygotes, relative to wild-type littermates (% Cyt-1, genotypes +/+: 38.66 ± 2.11 %, +/−: 20.712 ± 1.42 % and −/−: 0.00 ± 0.00 %; n=3, one-way ANOVA $F(2,6)=174.4$, ****$p<0.0001$), whereas relative levels of JM splice variants were unchanged (genotypes +/+: 18.16 ± 0.70%, +/−: 18.97 ± 0.52% and −/−: 21.27 ± 0.78%; n=3, one-way ANOVA $F(2,6)=5.725$, *$p=0.0407$). (***D***) Amounts of ErbB3 and ErbB4 receptor transcripts in forebrain, relative to GAPDH, are the same between wild-type, Cyt-1 heterozygote and KO mice (% ErbB3/GAPDH; +/+: 0.426 ± 0.004%, +/−: 0.423 ± 0.042% and −/−: 0.485 ± 0.054% and % ErbB4/GAPDH; +/+: 2.85 ± 0.09%, +/−: 2.90 ± 0.08% and −/−: 2.82 ± 0.05%; n=3, one-way ANOVA, $F(2,6)=0.2687$, $p=0.7731$ and n=3, one-way ANOVA, $F(2,6)=0.8039$, $p=0.4906$). (***E***) Relative ErbB3 and ErbB4 receptor transcript levels in the hippocampus are also unchanged between wild-type, Cyt-1 heterozygote and KO mice (% ErbB3/GAPDH levels; +/+: 0.138 ± 0.009%, +/−: 0.165 ± 0.012 % and −/−: 0.161 ± 0.002%; n=4, one-way ANOVA, $F(2,9)=2.67$, $p=0.1229$) and (% ErbB4/GAPDH; +/+: 0.801 ± 0.041%, +/−: 0.857 ± 0.015% and −/−: 0.975 ± 0.066%; n=4, one-way ANOVA, $F(2,9)=3.82$, $p=0.0628$).

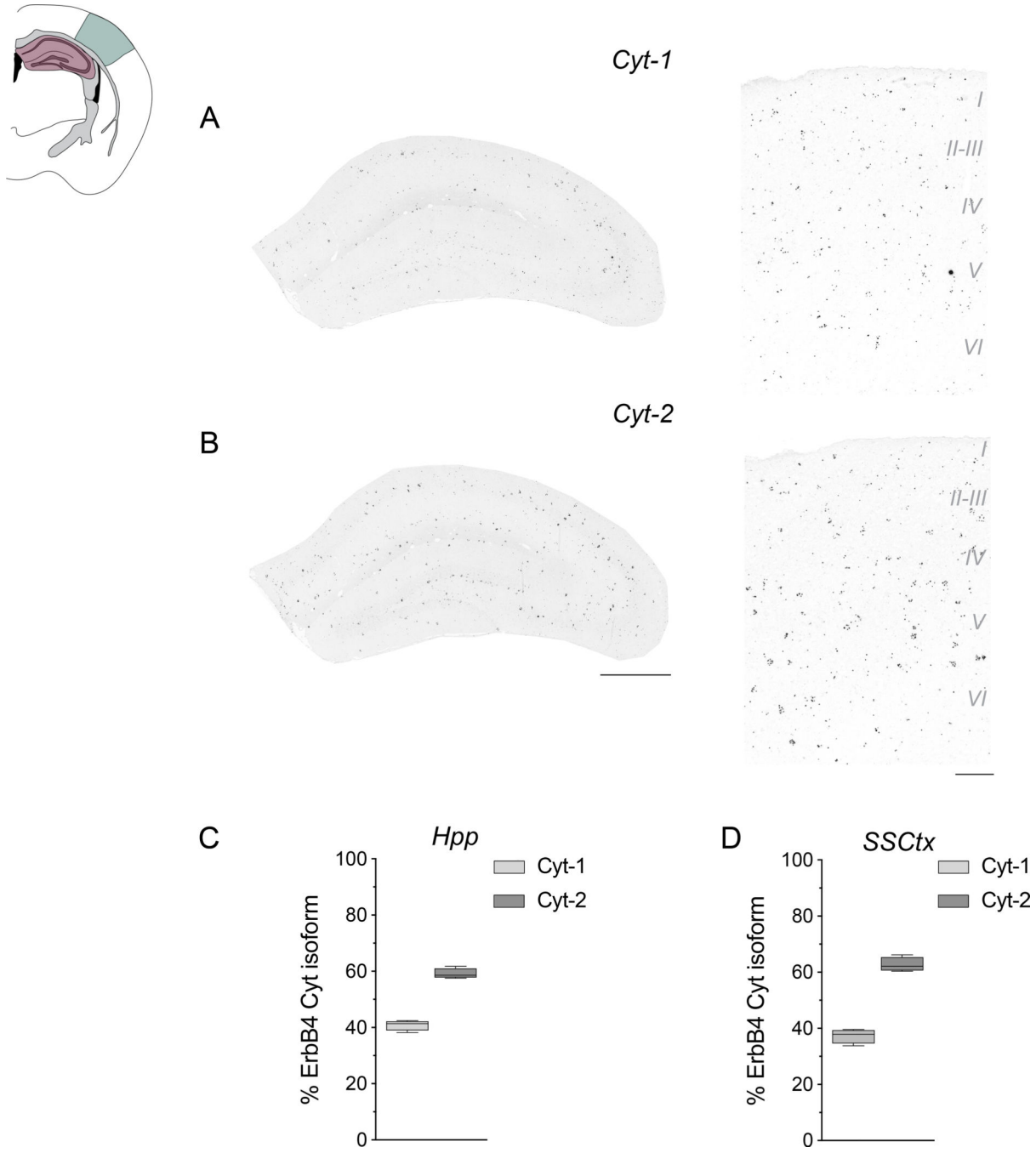

Figure 2. Expression of ErbB4 Cyt isoforms in hippocampal and cortical interneurons.

Expression of ErbB4 Cyt-1 and Cyt-2 splice variants was analyzed with exon-junction-specific ISH probes on coronal sections of adult mice using Basescope. A schematic of the coronal sections utilized is shown and highlights the approximate dorsal hippocampal (Hpp; *pink shade*) and primary somatosensory cortex (SSCtx; *green*) regions used for the analysis. ***A,B***) Representative results for (***A***) Cyt-1 and (***B***) Cyt-2 in the Hpp (*left*) and SSCtx (*right*). ***C,D***) Quantitative analysis of relative levels of Cyt splice variants in the Hpp (Cyt-1: 40.83 ± 0.9215%, Cyt-2: 59.17 ± 0.9215%, n=4; two-tailed Wilcoxon test, p=0.1250) and SSCtx

(Cyt-1: 37.28 ± 1.276%, Cyt-2: 62.72 ± 1.276%, n=4; two-tailed Wilcoxon test, p=0.1250). Scale bars 500 μm in B, 100 μm in D.

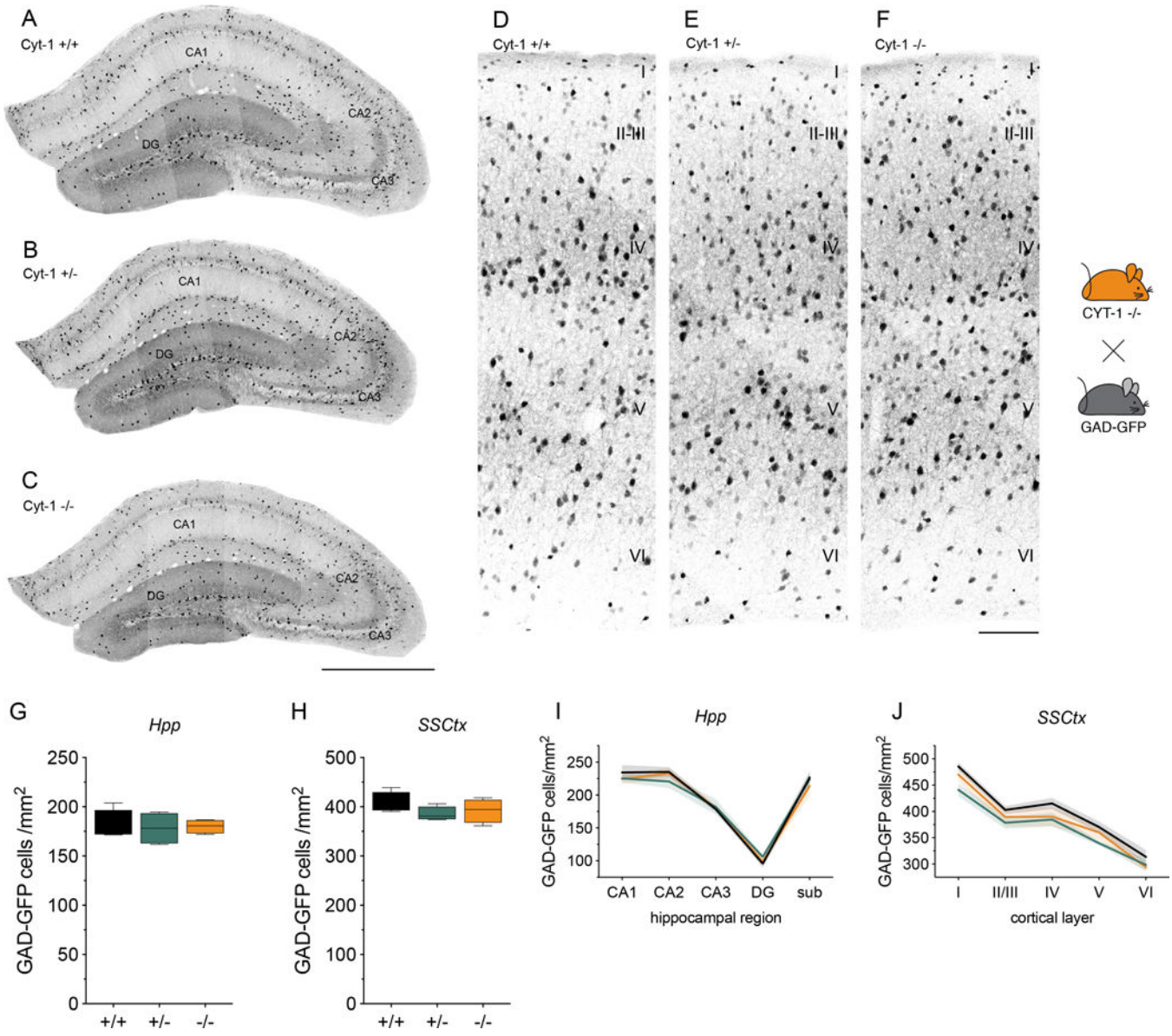

Figure 3. GABAergic interneurons in the hippocampus and primary somatosensory cortex are unaltered in Cyt-1 mutant mice.

Representative images of GFP-expressing GABAergic interneurons in the (***A-C***) dorsal hippocampus and (***D-F***) primary somatosensory cortex of control (***A,D***), Cyt-1 heterozygote (***B,E***), and KO (***C,F***) adolescent mice (P30). GABAergic neurons were labeled by breeding ErbB4 Cyt-1 KOs to transgenic GAD67-GFP mice (see Methods). Quantification of GFP-labelled GABAergic interneurons/mm^2 in the (***G***) hippocampus (genotypes +/+: 180.8 ± 7.73, +/−: 178.1 ± 8.21 and −/−: 180.1 ± 3.54 cells/mm^2; n=4, Kruskal-Wallis test, p=0.9410) and (***H***) in SSCtx (genotypes +/+: 407.7 ± 10.71, +/−: 385.5 ± 7.10 and −/−: 392.0 ± 11.99 cells/mm^2; n=4, one-way ANOVA F(2,9)=1.264, p=0.3283). ***I,J***) Graphs showing (***I***) the Hpp subregional and (***J***) SSCtx layer-specific distribution of GFP-labeled GABAergic interneurons in ErbB4 Cyt-1 KO (*orange*), heterozygote (*green*) and control

(*black*) mice (n=4; two-way ANOVA). Scale bars 500 μm in C, 100 μm in F. DG, dentate gyrus; sub, subiculum; CA1-CA3, cornu ammonis regions.

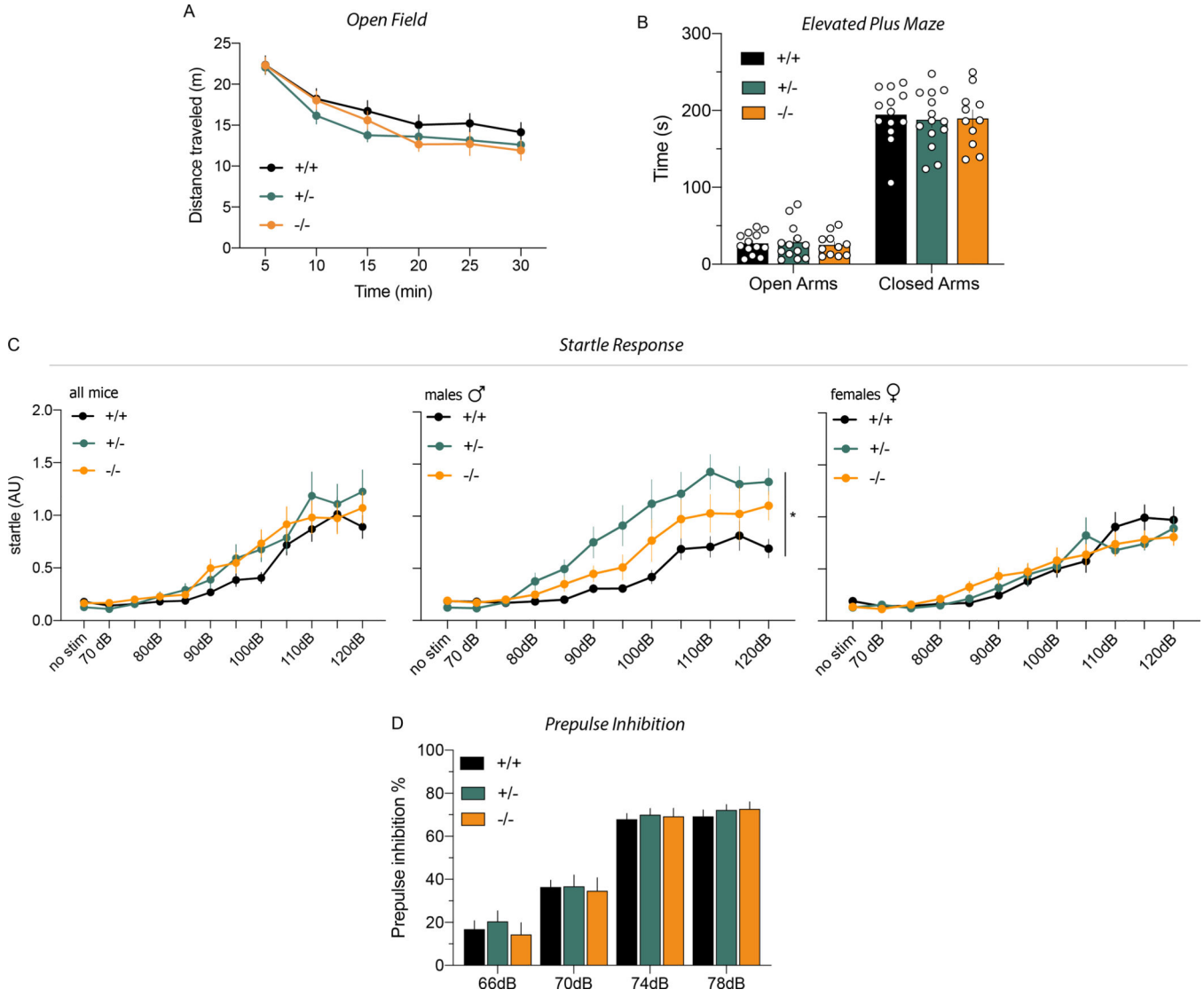

Figure 4. Behaviors altered in ErbB4 null mice are not affected in Cyt-1 KOs.

Performances on motor, affective (anxiety) and sensory-motor behavioral tasks known to be altered in ErbB4 null and PV-Cre; ErbB4$^{fl/fl}$ mice were analyzed in cohorts of adult Cyt-1 KO (*orange*), heterozygote (*green*) and control (*black*) mice. ***A***) Open field: mice showed similar habituation to a novel environment and total distance travelled in 30 min (genotypes +/+: 101.7 ± 6.2, +/−: 91.3 ± 3.8, −/−: 85.6 ± 2.4 meters, Welch's ANOVA, F(2,21.4)=3.197, p=0.0610, Dunnett's multiple comparisons test +/+ vs. −/− p=0.0791, +/+ vs. +/− p=0.4167, +/− vs. −/− p=0.5085; n=10–14/genotype). ***B***) Elevated plus maze: Cyt-1 KO, heterozygotes and control mice spent the same time (sec) in the open (genotypes +/+: 27.04 ± 3.87, +/−: 28.59 ± 6.41 and −/−: 25.07 ± 4.36) and closed (genotypes +/+: 194.5 ± 9.82, +/− 187.8 ± 9.81, −/− 189.7 ± 11.21; mixed-effects analysis, F(2,69)=0.1420, p=0.8679, 1 outlier value removed) arms of the plus maze. ***C***) Startle response (arbitrary units; AU) to increasing auditory stimuli intensities (70–120 dB) in both sexes (*left panel:* n=17–18/genotype, mixed-effects analysis, F(22,532)=1.191, p=0.2494,

10 outlier values removed), male ErbB4 Cyt-1 KOs only (*center panel*: n=8–9/genotype, mixed-effects analysis, F(2,23)=5.321, p=0.0126*), and female KO mice only (*right panel*: n=9/genotype, mixed-effects analysis, F(2,24)=0.01569, p=0.9844). ***D***) PPI: sensory-motor inhibitory responses were not significantly different between Cyt-1 KO, heterozygote and control mice (n=17–18/genotype, two-way ANOVA, F(2,49)=0.1582, p=0.8541).

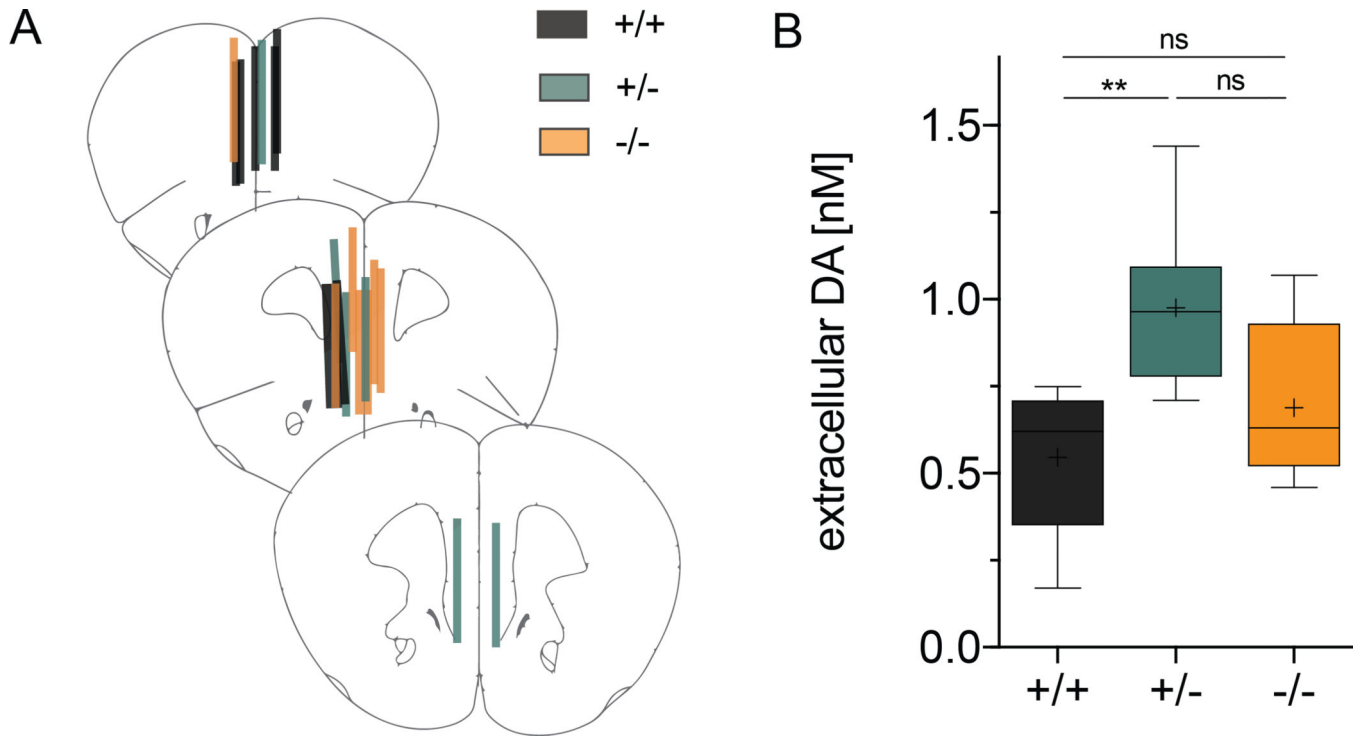

Figure 5. Tonic extracellular DA levels are increased in Cyt-1 heterozygote mice

Extracellular DA levels were analyzed by unilateral no-net-flux microdialysis in the mPFC of freely moving control (*black*), heterozygote (*green*) and Cyt-1 KO (*orange*) mice. (**A**) Verification of microdialysis probe placement in the mPFC at bregma levels +2.22 mm, +1.98 mm and +1.78 mm in 50 μm-thick sections using Nissl staining. (**B**) Measurements for tonic extracellular DA levels in the mPFC of Cyt-1 mutants and controls (+/+ 0.546 ± 0.080 nM, +/− 0.977 ± 0.103 nM, +/+ 0.689 ± 0.085 nM, n=6–7/genotype, one-way ANOVA, $F(2,17)=5.863$, *p=0.0116; +/+ vs. −/− p=0.4876, +/+ vs. +/− **p=0.0094, +/− vs. −/− p=0.089).

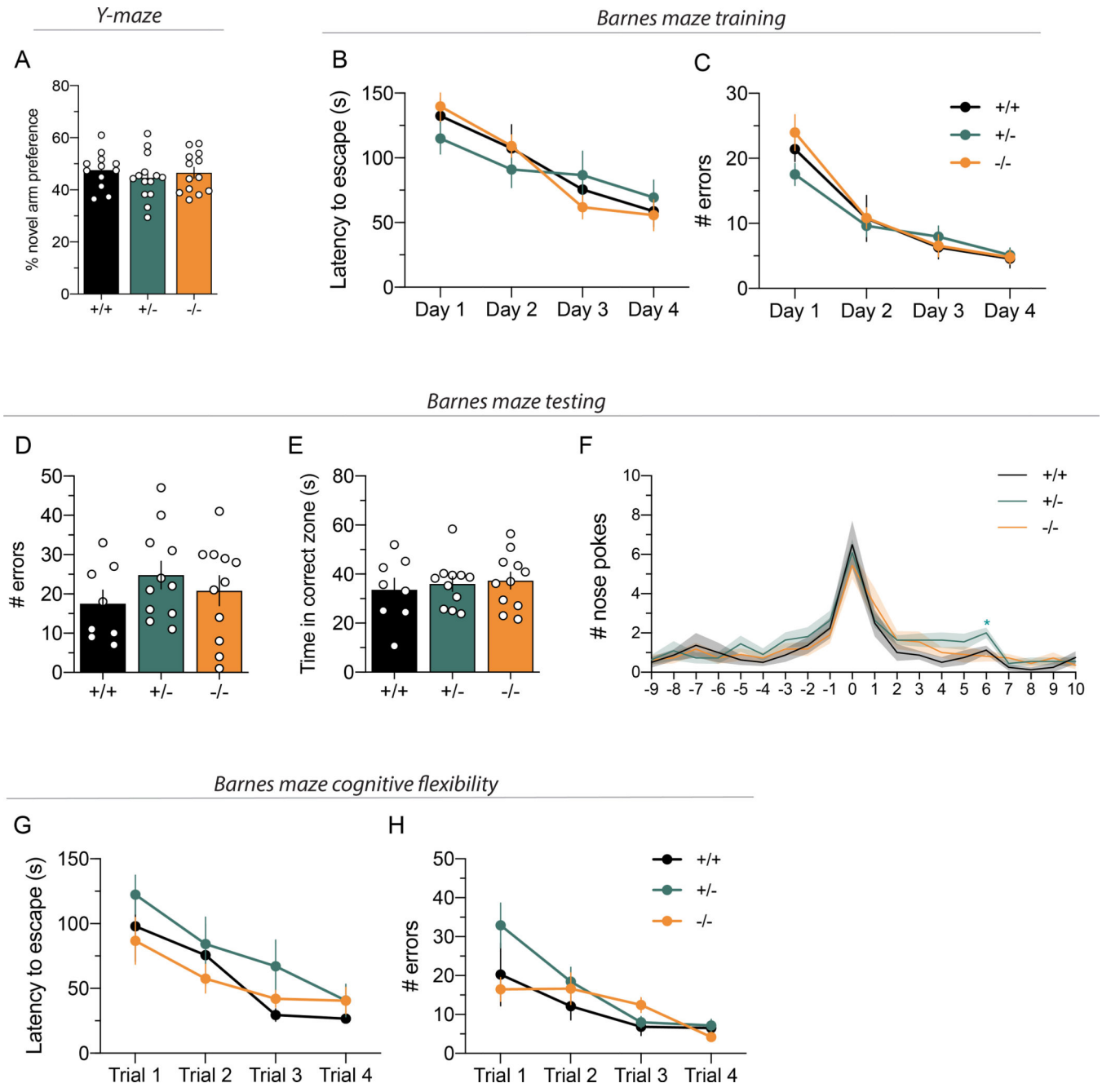

Figure 6. Cyt-1 mutant mice have normal working and reference memory, and cognitive flexibility.

(***A***) Working memory, plotted as percentage for novel arm preference in the Y-maze, is normal in Cyt-1 mutant mice (−/−; *orange*) compared to heterozygote (+/−; *green*) and wildtype (+/+; *black*) littermates (n=12–14/genotype, % alternation +/+ 47.58 ± 2.00%, +/− 44.66 ± 2.32%, +/+ 46.54 ± 2.12%, one-way ANOVA, F(2,36)=0.4677 p=0.6302). (***B-G***) Spatial reference memory of Cyt-1 KO mice in the Barnes maze is comparable to heterozygote and wild-type littermates during (***B,C***) initial training over four days, (***D-F***) testing on day five (n=8–11/genotype) and (***G***) adaption to a new target location. (***B***) Latency

to escape during training (n=8–11/genotype, two-way ANOVA, F(6,81)=1.580, p=0.1635). (***C***) Number of errors committed during training (n=8–11/genotype, mixed-effects analysis, F(6,80)=1.158, p=0.3373). (***D***) Number of errors during testing (+/+: 17.5 ± 3.5, +/−: 24.8 ± 3.5, −/−: 20.8 ± 3.8, one-way ANOVA, F(2,27)=0.9498, p=0.3994). (***E***) Time spent in the correct quadrant/zone during testing (+/+ 33.6 ± 4.7 s, +/− 36.0 ± 3.0 s, −/− 37.4 ± 3.4 s, one-way ANOVA, F(2,27)=0.2508, p=0.7799). (***F***) Nose pokes in individual holes during testing (0 – target, 10 – opposite; two-way ANOVA (no outlier exclusion), F(38,513)=0.8407, p=0.7396, Tukey's multiple comparisons test main column effect, +/+ vs. +/− p=0.1450, +/+ vs. −/− p=0.8096, +/− vs. −/− p=0.3263) (***G***) Latency to escape (n=8–11/genotype, mixed-effects analysis, F(6,79)=0.5949, p=0.7335, 2 outlier values) and (***H***) number of errors after moving target to a new position (cognitive flexibility; n=8–11/genotype, mixed-effects analysis, F(6,78)=1.906, p=0.0903, 3 outlier values removed).

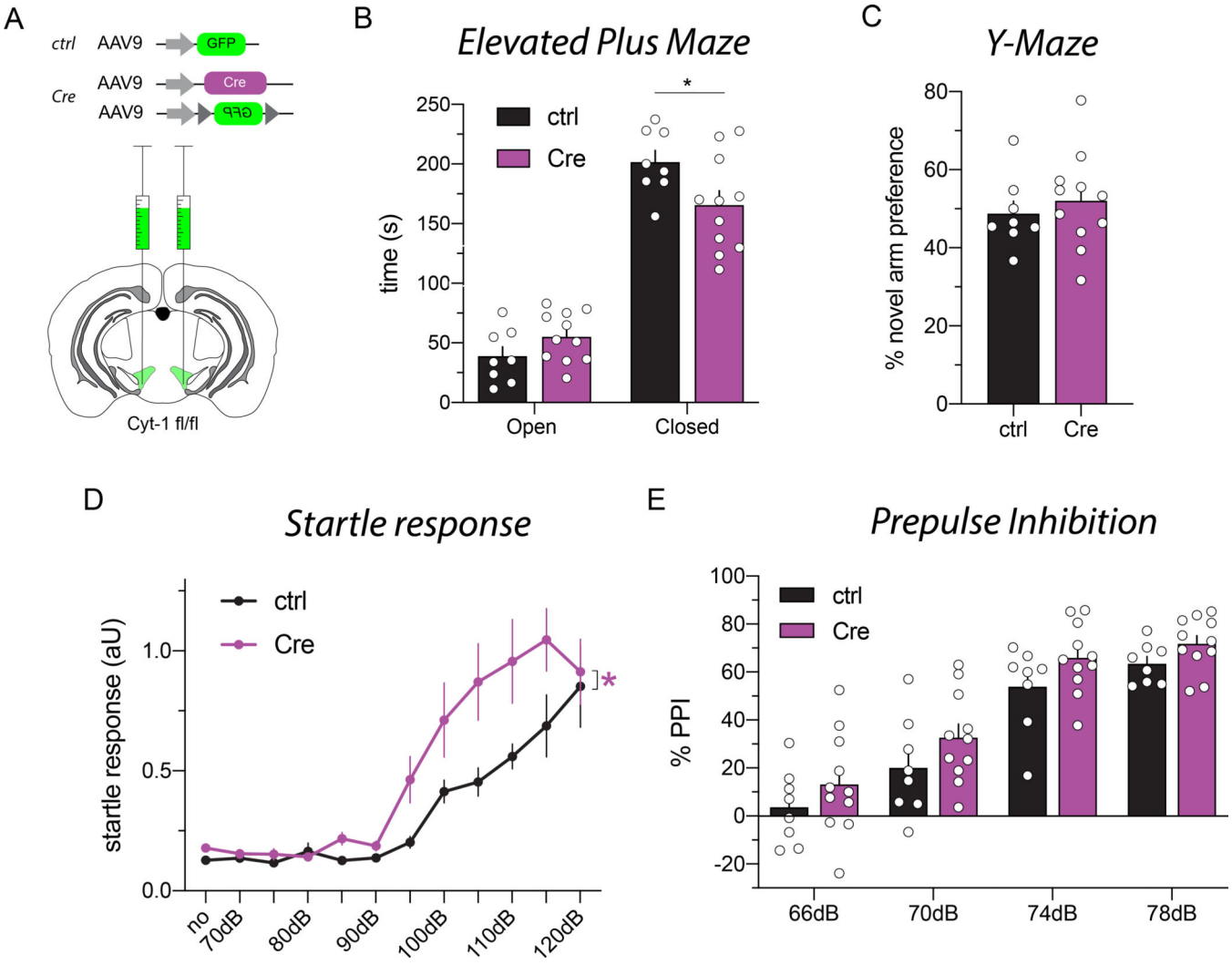

Figure 7. Deletion of the Cyt-1 exon in the VTA of adult mice results in behavioral abnormalities.

(***A***) Illustration of adeno-associated virus (AAV) injections into the VTA of ErbB4 Cyt-1$^{fl/fl}$ mice used to generate controls (AAV9-hSynI-GFP) and acute Cyt-1 KOs (AAV9-hSynI-Cre & AAV9-hSynI-DIO-GFP). (***B-E***) Controls (n=8) and acute Cyt-1 KOs (n=11) were tested in different behavioral paradigms. (***B***) Acute Cyt-1 KOs spend less time in closed arms of the elevated plus maze (two-way ANOVA, F(1,17)=4.421, p=0.0507, Sidak's multiple comparison test ctrl vs. Cre, closed arms p=0.0234*, open arms p=0.4123). (***C***) No differences were found between cohorts in the Y-maze (unpaired two-tailed t-test, p=0.5380). (***D***) Acute Cyt-1 KOs exhibit an enhanced startle response relative to controls, (mixed-effects analysis, F(11,181)=1.874, p=0.0454*, ctrl vs. Cre p=0.0490*; 6 outlier values from a total of 209 values in 5 mice); however, (***E***) PPI does not differ between cohorts, (two-way ANOVA, F(3,51)=0.09446, p=0.9628, ctrl vs. Cre p=0.0601).